1. INTRODUCTION

The present investigation of long slender cylinders in axial and near axial flow was motivated by the current interest in the fluid flow over towed sonar arrays. Such arrays are used to locate and identify underwater vehicles by the analysis of sound recordings obtained from the hydrophones (underwater microphones) in the array. Means are needed by which the fluid flow over the sleeve containing the microphones and associated cables may be analysed to improve the discrimination between the noise generated by the movement of the microphone array itself and that generated by distant underwater vehicles or other noise sources.

The problem in terms of fluid mechanics is to describe the fluid flow over long circular cylinders in both axial flow and at small angles of yaw, with the intention of identifying any larger scale flow processes in either the cylinder boundary layer, or in the wake therefrom, which occur at frequencies lower than that of the fine scale turbulence (of order 10 kHz). Regular periodic processes are of particular interest. This requires an extension of the current understanding of cylinder wakes to include very small yaw angles, and an extension of the current understanding of turbulent boundary layers to include cases of very long cylinders in axial and near axial flow.

On the basis of results obtained in their experimental investigation of thick turbulent boundary layers on very long cylinders in axial flow, Luxton et al. (1984) suggested that the stripping of retarded inner-layer fluid from the cylinder by turbulent cross-flows, accompanied by the generation of high instantaneous velocity gradients at the cylinder surface, could be responsible for the high levels of vorticity production

necessary for the small cylindrical surface area to sustain the large volume of turbulence surrounding it. This volume of turbulence, per unit of surface area, may be an order of magnitude or more greater than that in a flat-plate boundary layer. The requirement for higher levels of vorticity production in a thick axisymmetric turbulent boundary layer than in a flat-plate layer also leads to the expectation of higher wall shear stresses in the axisymmetric case, and experimental results such as those of Willmarth and Yang (1970), Willmarth et.al.(1976), Lueptow et.al.(1985), Lueptow and Haritonidis (1987), and Cipolla and Keith (2003a, 2003b) are in accord with this expectation.

In later work by Bull et al.(1988), additional support for this hypothesis came with preliminary evidence suggesting the existence of propagating fronts of low speed fluid in the boundary layer. This, in turn, raised the possibility that stripping of retarded fluid from the cylinder might be associated with localised vortex shedding being induced by turbulent cross-flows.

The effects of such cross-flows have been interpreted by Lueptow and Haritonidis (1987) in terms of the burst-sweep mechanism of turbulence generation identified in planar boundary layers, with modification for transverse curvature. It is proposed here that the cross-flow effects in the boundary layer on a slender cylinder in axial and near-axial flow constitute a different, and possibly dominant, turbulence generation mechanism from that characterising planar boundary layers. As a consequence, an investigation was undertaken of vortex shedding from cylinders yawed at small angles from the flow direction, and of the turbulence mechanisms within the axisymmetric boundary layer formed at zero yaw.

The investigation of vortex shedding from a yawed cylinder is to determine the Reynolds-number and yaw-angle regimes where vortex shedding occurs, and to determine the frequency f and orientation α of the vortices as a function of the cylinder geometry and the flow state. The cylinder geometry is defined by the three variables: diameter d, location x along the overall length l, and yaw angle β.

The flow state is defined by three parameters, the free stream velocity U_1, the fluid density ρ and the fluid viscosity μ. Thus the overall condition of the flow over a cylinder shedding vortices at an angle α, and a frequency f may be described by the set of variables { d, x, β, U_1, ρ, μ, α, f }. For a particular cylinder / fluid combination, experiments have been performed to measure the vortex shedding frequency and orientation while the flow velocity and yaw angle are varied to obtain a relationship of the form:

$$f = \text{function}(U_1, \beta, x), \qquad [1.1\ a]$$

$$\alpha = \text{function}(U_1, \beta, x). \qquad [1.1\ b]$$

These dimensional forms may be generalised to collapse data from a variety of cylinder-geometry / fluid-velocity combinations by forming non-dimensional parameters from f, U_1, β and x. The velocity U_1 is non-dimensionalised as a Reynolds number

$$Re_d = \rho U_1 d/\mu = U_1 d/\nu \qquad [1.2]$$

or $$Re_a = \rho U_1 a/\mu = U_1 a/\nu ,$$

based on diameter or radius, and the periodic vortex shedding frequency may be non-dimensionalised as

$$F = \rho f d^2/\mu = f d^2/\nu . \qquad [1.3]$$

An alternative to the non-dimensional frequency parameter F is the Strouhal number St, where $St = F/Re_d = fd/U_1$. Although the use of Strouhal number is more common, the use of F allows the effects of frequency and flow velocity to be separated.

The yaw angle is itself non-dimensional, but may also be expressed as a trigonometric function such as sin β, which may be interpreted physically as the ratio of the cross-flow velocity component to the total free stream velocity. The orientation of the vortex line to the cylinder axis α is also non-dimensional, and expresses the ratio of the axial to normal vorticity generated by the cylinder. The length x may be non-dimensionalised as the length-to-radius ratio x/a, a measure of the "slenderness" of the cylinder, or as a Reynolds number based on length:

$$Re_x = \rho U_1 x/\mu = U_1 x/\nu \ . \qquad [1.4]$$

Thus the formal relationships, in terms of non-dimensional parameters, are

$$F = \text{function}(\ \beta,\ Re_d,\ x/a\ ) \qquad [1.5\ a]$$

and $$\alpha = \text{function}(\ \beta,\ Re_d,\ x/a\ ). \qquad [1.5\ b]$$

The non-dimensional frequency F can be expected to vary with x/a as the thickness of the cylinder boundary layer increases (implying that vortex cells are formed in the flow), an effect which will decrease as the yaw angle increases. In the extreme case of $\beta = 90°$ the axial velocity component approaches zero and the flow becomes independent of x. For the small yaw angles and very large x/a considered here, the flow is only weakly dependent on x/a as the axial flow is well developed.

Similarity analysis of the mean flow within planar turbulent boundary layers (Coles 1955,1956,1957) indicates the presence of inner and outer layer regimes. The inner layer regime is scaled on the friction velocity U_τ, defined in terms of the wall shear stress as $U_\tau = \sqrt{(\tau_w/\rho)}$. The normalised local non-dimensional velocity and distance from the wall are then expressed in "wall units" as $U^+ = U/U_\tau$ and $y^+ = yU_\tau/\nu$ respectively. The outer layer regime is scaled on the free stream velocity U_1 and the boundary layer thickness δ. Thus the non-dimensional parameters for velocity and position in this region are U/U_1 and y/δ respectively.

The addition of the transverse curvature, characterised by the cylinder radius a, for the axisymmetric boundary layer introduces two new non-dimensional parameters. These are the ratios of the length scales of each of the inner and the outer layers to the radius of transverse curvature. Thus for the inner layer length scale, ν/U_τ, the ratio becomes ν/aU_τ, that is $1/a^+$, where $a^+ = aU_\tau/\nu$, and for the outer length scale δ the ratio becomes δ/a.

The investigation of the effects of transverse curvature on the mechanisms of turbulence production within the thick axisymmetric boundary layer formed at zero yaw angle ($\beta = 0°$) examines the case where the curvature is large in comparison with both the inner and outer length scales. This requires small a^+ and large δ/a. As a^+ is proportional to Re_a (Luxton et.al.1984) and δ increases with x, this means small Re_a and large x/a. The investigation demonstrates the occurrence of cross flows of boundary layer fluid over the cylinder, which result in fluid being removed from the inner regions of the boundary layer to form fronts of low speed fluid which extend across the boundary layer radius. This process is found to be repeated continuously but aperiodically.

The form of this axisymmetric boundary layer may be described by the momentum integral equation (Equation [1.6] below) which is obtained by the integration of the equation of motion of the boundary layer from the cylinder surface to the outer edge of the boundary layer.

The momentum integral equation is expressed in terms of a momentum thickness θ_2 (Equation [1.7] below), and a displacement thickness δ_2^* (Equation [1.8] below) as

$$(1 + \frac{\theta_2}{a}) \frac{d\theta_2}{dx} + \frac{1}{U_1} \frac{dU_1}{dx} \theta_2 (1 + \frac{\theta_2}{2a}) (H_2+2) = \frac{\tau_w}{\rho U_1^2} \quad , \qquad [1.6]$$

where

$$(\theta_2 + a)^2 - a^2 = \int_a^{a+\delta} \frac{U}{U_1} \left[1-\frac{U}{U_1}\right] 2rdr \quad , \qquad [1.7]$$

$$(\delta_2^* + a)^2 - a^2 = \int_a^{a+\delta} \left[1-\frac{U}{U_1}\right] 2rdr \quad , \qquad [1.8]$$

and

$$H_2 = \frac{\delta_2^* (1+\frac{\delta_2^*}{2a})}{\theta_2(1+\frac{\theta_2}{2a})} \quad .$$

Equation [1.6] shows that $d\theta_2/dx$ will be positive for a non-zero wall shear stress τ_w and zero pressure gradient (ie. $dU_1/dx = 0$); thus the boundary-layer thickness will continue to increase with increasing values of x. For the current experiments at

$x/a = 6000$, the ratio of boundary layer thickness to cylinder radius δ/a can be as high as 50. The results of Luxton et al.(1984) show that for boundary layers with $Re_{\theta 2}$ in the range 1000 - 3000 and Re_a and a^+ as low as 140 and 13 respectively the layer is fully turbulent. They show, further, that, as x/a becomes large ($x/a > 5000$, $\delta/a >> 1$), the shape of the axisymmetric boundary layer approaches a state of similarity and the rate of boundary-layer growth becomes very small. The current experiments, conducted at $x/a = 6000$ with $2000 < Re_{\theta 2} < 3000$, Re_a in the range 300 - 600 and a^+ in the range 22 - 41, can therefore safely be assumed to be representative of the fully-developed boundary layer in its asymptotic form.

1.1 Aims of the Research Program.

The aim of the research program is to advance the current understanding of the flow processes characterising a long slender cylinder in axial and near axial flow. As described in the following chapters, this is achieved by an experimental investigation of the flow by means of velocity measurement and flow visualisation. In the axial flow case, the resultant thick axisymmetric turbulent boundary layer is examined to determine both the mean and statistical properties of the turbulent flow. From these measurements the characteristics of the boundary layer are compared with the well established case of the flat plate boundary layer, and also with the axisymmetric boundary layer with smaller δ/a, which is the subject of current research by other investigators, (see, for example, Bokde, Lueptow and Abraham 1999).

Further investigation of the axisymmetric boundary layer to determine the character of the fronts of low speed fluid, thought to be associated with large negative spikes observed in the time series records of the turbulent velocity fluctuations, is described. Experiments to determine the flow mechanism by which these fronts are formed are discussed, and a description of the associated turbulence generation process is formulated to explain how, and why, this type of boundary layer differs from both the flat plate and the small δ/a axial-cylinder cases.

For the near axial flow case, the asymmetry of the turbulent boundary layer has been measured for very small yaw angles in order to determine the geometric limits within which the prior results for the axisymmetric boundary layer may reasonably be

applied. For larger yaw angles, greater than one degree, the occurrence of regular vortex shedding is examined. The regime of flow within which regular vortex shedding occurs is determined, and measurements of the vortex shedding frequency within this regime are presented. From these measurements the characteristic relationship between the vortex shedding frequency, the cylinder geometry and the properties of the fluid flow is determined in terms of non-dimensional parameters.

2. LITERATURE REVIEW

Previous research on circular cylinders in axial and near-axial flow has been conducted in two major fields: the analysis of the boundary layer and mechanisms of turbulence production, and the analysis of the vortex shedding behaviour.

The vast majority of the relevant boundary layer research seeks to modify flat-plate boundary layer theory to account for the effects of transverse curvature to provide a description of the axisymmetric boundary layer generated on a cylinder for $\delta/a \leq 5$. The knowledge of mean boundary layer properties has been extended to account for the effect of yawing the cylinder from the axial case. The mechanism of turbulence production in such flat-plate and axisymmetric boundary layers has yet to be fully understood, and is the subject of a large volume of current research. The effects of increasing δ/a and possible cross-flows within the boundary layer on the mechanisms of turbulence production in thick boundary layers have yet to be explained for $\delta/a >> 1$ for cylinders in axial and near-axial flow. Such considerations have stimulated the present investigation of turbulence production in thick axisymmetric boundary layers.

Vortex shedding in the wake of cylinders which are orientated transversely to the flow direction is well known. When the flow is other than normal to the cylinder axis, the 'normal' vortex shedding theory must be modified to account for the effect of yaw. While data on vortex shedding from near-normal cylinders abounds, no previous research has been found to extend the yaw angle beyond 76° from the normal, which corresponds to an angle relative to the cylinder axis of $\beta = 14°$. At the other end of

the scale Luxton et.al.(1984), Lueptow et.al.(1985,1986,1987) and Cipolla and Keith (2003a,2003b) have studied flows along slender cylinders aligned with the flow direction. The present experimental investigation seeks to 'close the gap' between these two families of experiments by studying the vortex shedding from cylinders in near-axial flow.

2.1 Turbulent Boundary Layers.

Initial methods to describe boundary layer turbulence were based on the characterisation of flat-plate turbulent boundary layers in terms of the flow parameters and the production and dissipation of energy within the layer. Townsend (1956) provides the basis for this analysis by considering the boundary layer to be composed of two distinct parts, an inner layer wholly controlled by the local wall stress, and an outer layer with wake-like properties. Analytical descriptions of the mean boundary layer properties within these two regions have been developed by similarity analysis to identify the relevant scaling parameters, and by the application of the concepts of "the law of the wall" [Coles(1955)] for the inner region, and "the law of the wake" [Coles(1956,1957)] for the outer region. Early analytical models of the structure of turbulence by Theodorsen (1952, 1955) identify the "horseshoe" vortex, and a series of smaller "horseshoe" vortices formed over the surface of the primary vortex, as the principal coherent structures within a turbulent boundary layer. The further analysis of the fundamental mechanisms by which these turbulence processes occur has progressed largely by experimental investigations spanning the whole class of shear flows.

Correlation measurements of fluctuating velocities and wall pressures by Wooldridge and Willmarth (1962) lead to their hypothesis that the measured vector field of the pressure-velocity correlation data can be represented by a velocity field generated by the superposition of a spectrum of eddies whose axes are perpendicular to the mean velocity, in a plane parallel to the wall, which interfaces with a layer of fluid near the wall. Flow visualisation studies by Kline et.al. (1967) reveal the presence of

low speed streaks in the near-wall region. These were observed to interact with the outer layer by a process of gradual 'lift-up', followed by sudden oscillation, bursting, and ejection, leading to the hypothesis that these processes are an important mechanism in the generation and transport of turbulence within the boundary layer.

Visual investigations by Corino and Brodkey (1969) of pipe flow boundary layers also detected the ejection of fluid elements from the wall region, and identified the interaction of this process with the mean flow as an important factor in the creation of turbulence. The initial analysis of the frequency of these inner-layer events, termed 'bursts' by Rao et.al. (1971) and by Laufer and Narayanan (1971), suggests that the mean frequency of the bursts scales with the outer-layer variables, and that the mechanism can thus best be explained in terms of a coupling between the inner and outer layers.

Further investigations of the wall region by Blackwelder and Kaplan (1976) confirm that, although the bursting process has its largest effect near the wall and, although its vertical extent scales on the inner-layer variables, its frequency of occurrence scales on the outer-layer variables. However, further analysis of the bursting frequency by Blackwelder and Haritonidis (1983) led to the conclusion that the mean frequency really scales with the inner-region variables. These authors attributed the previous findings of outer-region scaling to the effects of spatial averaging over the sensor length. Subsequent examinations by Alfredsson and Johansson (1984 a) found that the governing time scale for events in the near-wall region is a mixture of both inner and outer time scales. The work of Wark and Nagib (1991) indicates that a hierarchy of burst-event sizes exists. They suggest that the time scales are generated by

a wall-layer mechanism but grow to scales and are convected with velocities determined by the outer layer.

The relative importance of these burst events in the production of turbulence has been determined by Willmarth and Lu (1972) by conditional sampling of the u and v velocity components. These measurements indicate that the contribution of the bursting process to the Reynolds stress and to the turbulent energy production in the near-wall region occurs intermittently, and is of relatively large magnitude and of short duration. Flow visualisation of the bursting process by Nychas et.al. (1973) confirms the importance of the process in the production of turbulence and additionally shows that the recovery process, termed "sweeps", also makes positive contributions to the Reynolds stress. A model of the burst-sweep process was proposed by Offen and Kline (1975) envisaging wallward "sweeps" of fluid, caused by large scale eddies, generating pressure gradients that are sufficiently adverse to lift low speed streaks of fluid up from the wall ("bursts"). New low speed streaks are then formed downstream by fluid elements from the burst returning to the wall and being decelerated by viscous forces. The process can loosely be described as a sequence of intermittent 'internal separations' within the turbulent boundary layer.

The spanwise structure of the burst mechanism near the wall examined by Blackwelder and Eckelmann (1977,1979) suggests the existence of a system of counter-rotating streamwise vortices which are disturbed intermittently by high speed sweeps. These streamwise vortices "pump" fluid away from the wall, thus forming low speed streaks which are eventually terminated by a sweep. Measurements by Willmarth and Bogar (1977) also support the proposition of streamwise vorticity as the mechanism for

producing intermittent small scale disturbances in the near wall flow. Ensemble averages of the conditionally-sampled turbulent velocity fluctuations by Wallace et.al. (1977) show a characteristic gradual deceleration of the u component followed by a strong acceleration, in agreement with the burst-sweep model.

Analysis of the large scale outer layer structures by Thomas (1977), Brown and Thomas (1977) and Thomas and Bull (1983), suggests the existence of organised structures on the scale of the full boundary layer, in the form of oblique fronts of fluid which they postulated to be the initiators of the wall region events. A visual study of such coherent structures by Praturi and Brodkey (1978) supports this concept of the outer-layer structure driving the inner-layer events. Further evidence for the formation of oblique fronts is provided by Kreplin and Eckelmann (1979), who postulate that the fronts originate from the inclined streamwise vortices. The spanwise structure of the bursts and sweeps measured by Antonia and Bisset (1990) indicates that the sweeps are approximately 25% wider than the bursts, and are twice as long in the streamwise direction.

An examination by Morrison et.al. (1992) of ejections and sweeps detected by conditional sampling of experimental velocity data indicates that the interaction of the inner and outer layers is controlled principally by the ejections from the inner layer. The results of experimental emulation of turbulent-boundary-layer eddy structures, conducted by Myose and Blackwelder (1994), indicate that the outer region of the turbulent boundary layer also plays a role in the bursting process. The analysis of numerical simulations of transitional and turbulent boundary layers by Rempfer and Fasel (1994 a,b) suggest the possibility of determining the structure of turbulence as a

non-linear interaction, perhaps involving only a small number of coherent structures.

The merits of the various sampling and averaging techniques used in detecting turbulent structures are compared by Subramanian et.al. (1982) with the conclusion that multiple point rake detection schemes are preferable to single point measurement methods. The addition of pattern recognition to single point detection schemes by Blackwelder (1977) increases the effectiveness of simple conditional sampling techniques by suppressing the effects of the random phase which occurs between spatially or temporally separated signals. Zaric's (1982) method of pattern recognition however improves the single point method to a similar level by using a more complex event detection scheme based on the separate detection of both a burst and a sweep rather than detection of a complete sweep pattern. The merit of this method is also demonstrated by combined flow visualisation and hot-wire anemometry analysis of the flow by Zaric et.al. (1984). The advantages of combined flow visualisation and anemometry are further demonstrated by Wei et.al. (1984) in examining individual large scale events without the possible loss of information resulting from any averaging process.

A comparison by Alfredsson and Johansson (1984 b) of the *uv*-quadrant method of analysis with the variable interval time averaging (VITA) technique suggests that similar results may be obtained by both methods provided that suitable VITA detection criteria are used. A more extensive comparison by Bogard and Tiederman (1986) of various detection schemes and flow visualisation results found that the quadrant technique provides the greatest reliability, and provides a high probability of detecting fluid ejections and a low probability of recording false detections. In Nagano and

Tagawa's (1995) study the u,v quadrant scheme has been further developed into a trajectory analysis technique (TRAT) designed to evaluate a fluid motion (turbulence structure) rather than to detect events only.

Various mechanisms have been advanced to explain the overall burst-sweep process. Falco (1982, 1983), proposed a turbulence model based on a vortex ring formed in the outer layer, which then approaches the wall at an acute angle. Initially behaving as a three-dimensional sweep, the ring appears as two upwardly inclined streamwise vortices as it interacts with the wall, producing the burst of ejected inner layer fluid. Smith and Metzler (1983) examined the formation and origin of 'stretched vortex loops', also referred to as 'hairpin vortices', as a mechanism for the formation of low speed streaks. This mechanism of vortex stretching as a source of turbulence production is also supported by the theoretical analysis by Coles (1984).

Theoretical models for near-wall turbulence are proposed by Haritonidis (1989), based on a modified mixing length hypothesis, and by Landahl (1990), based on a quasi-laminar model. These determine the characteristics of the turbulence resulting from a given burst geometry. The origin of the bursts suggested by Landahl (1990) lies in the formation of the streaky structure in the sub-layer. Such streaks grow from any initial local three-dimensional disturbances that have a non-zero net vertical momentum along lines of constant y,z (Landahl 1980). These disturbances could be initiated by any local inflectional instability region with spanwise asymmetry, such as an oblique wave-like disturbance which may result from a cross-flow instability induced by a large-scale spanwise motion (Landahl 1975). A theoretical model for the distribution of streamwise turbulence intensity has been formulated by Marusic et.al.(1997) based on the attached-

eddy model developed by Perry and Marusic (1995) and Marusic and Perry (1995).

The currently unsolved central issues in 'understanding' coherent boundary-layer motions are identified by Robinson (1991) as *(a)* vortex formation and evolution, and *(b)* interaction between coherent motions in the inner and outer regions of the boundary layer. Any model of coherent structures in the turbulent boundary layer must address both of these points, and also the Reynolds number dependence of the mechanisms involved, if it is to be generally applicable. Such a model has been suggested by Falco (1991) following a review of the many coherent motions detected previously, and consequent formulation of a proposed interaction mechanism and its Reynolds number dependence.

The successful identification of the attached vortex loops, envisaged by Theodorsen (1955), within the numerically simulated data for a flat plate turbulent boundary layer by Chong et.al.(1998), indicates that future studies of coherent structures within boundary layer turbulence may be conducted with some reliability by examining numerically-generated data.

The successful application of hydrogen-bubble flow-visualisation to the investigation of near-wall streamwise vortices and the associated fluid ejections in a flat plate boundary layer with mild streamwise curvature by Flack (1997) indicates the effectiveness of this technique for flat plate boundary layers with a simple three-dimensional aspect. It also suggests that the technique may be useful in the further study of coherent structures within turbulent boundary layers with stronger transverse curvature.

2.2 Boundary Layers on Cylinders Aligned with the Flow.

The current research is concerned with the very thick turbulent layer and the flow mechanisms which sustain it. Previous investigations have been conducted over a large range of Reynolds number (Re_a) and relative boundary layer thickness (δ/a) for both laminar and turbulent boundary layers.

Early analytical investigations of axisymmetric boundary layers by Seban and Bond (1951), Kelly (1954), Glauert and Lighthill (1955) and Cooke (1957) were restricted to the analysis of laminar flows. They produced results which described axisymmetric laminar boundary layers in terms of thickness and mean velocity profiles. The accuracy of these results has subsequently been improved by Curle (1980). This early analytical work was extended by Eckert (1952) to include turbulent boundary layers; however, the assumptions then made, in the absence of experimental results, on the effects of transverse curvature are now recognised as being inadequate.

Experimental measurements of the mean turbulent boundary layer properties by Richmond (1957), Yu (1958), Yasuhara (1959), Willmarth and Yang (1970) , Rao and Keshaven (1972) and Afzal and Singh (1976), have been compiled by Luxton et.al. (1984) by plotting the values of Re_a against a^+ for each data set, and by noting the corresponding values of δ/a and whether the velocity profile data match the inner-layer characteristics (an identifiable logarithmic region in the velocity profile) of the two-dimensional flat-plate boundary layer. This data compilation indicates that for values of $\delta/a \leq 5$ the mean properties of the axisymmetric layer are similar to the two-dimensional flat-plate layer, but that as δ/a is increased and a^+ decreased, the

properties of the axisymmetric layer progressively depart from the two-dimensional model. (It should be noted that the designations of the ordinate and the abscissa of figure 1 of Luxton et.al.(1984) should be interchanged.)

Based on this analysis, with the addition of their own experimental results, Luxton et.al.(1984) show that, if transverse curvature is to affect both the inner and outer layers, both the inner and outer characteristic length scales must be large compared with the transverse radius of curvature. Hence a^+ must be small and δ/a large, which requires that Re_a is small and Re_x is large. As $Re_x = (x/a)Re_a$, the requirements for significant effects of transverse curvature on both the inner and outer layer are then that x/a is large and that Re_a is small. At the stage where δ/a exceeds a value of about 20 and a^+ falls below about 200, both the outer and inner layers show marked effects of transverse curvature. In the present experiments, $\delta/a > 30$ and $a^+ < 41$, in which case curvature can be expected to affect the whole of the axisymmetric boundary layer.

The regime of essentially two-dimensional boundary layers (large Re_a, large a^+ and δ/a of order unity) has been the subject of numerous theoretical analyses. Afzal and Narasimha (1976) determined that the mean velocity distribution is logarithmic based on the method of mutual asymptotic expansions. This result is in agreement with the early experimental results compiled by Luxton et.al.(1984) for small δ/a. Modifications to the law of the wall have been proposed by Richmond (1957), based on Coles (1955) streamline hypothesis; and by Rao (1967) with supporting analysis by Chase (1972), White (1972) and Ackroyd (1982),in agreement with the experimental results of Rao and Keshaven (1972) and Willmarth et.al.(1976). The thick boundary layers on bodies

of revolution in the presence of a significant pressure gradient have been examined experimentally by Patel et.al.(1974) and Kegelman et.al.(1983). The results are in agreement with a numerical (k,ϵ) model calculated by Markatos (1984).

Mean velocity profiles and expressions for wall shear have also been obtained by solving the equations of motion using mixing length closures and numerical techniques [Sparrow et.al.(1963), Cebeci (1970), White et.al.(1973), Patel (1973) and Denli and Landweber (1979)], and by the extension of Head's (1958) entrainment theory by Shanebrook and Sumner (1970) to include transverse curvature. The calculation of mixing lengths and eddy viscosities by Lueptow et.al.(1985) and by Lueptow and Leehey (1986), using a constant eddy viscosity closure, and by Granville (1987) in a classical similarity-law analysis of the mixing length, currently enables the axisymmetric turbulent boundary layer velocity profiles to be calculated with some accuracy in the $\delta/a \leq 5$ regime. However the effects of transverse curvature on the mechanisms of turbulence production involved in such layers, particularly at larger δ/a, are not yet fully understood.

The earliest indications of the effects of transverse curvature on the structure and mechanisms of turbulence derive from the measurements, by Willmarth and Yang (1970), of wall-pressure fluctuations beneath turbulent boundary layers on both flat plates and cylinders [$\delta/a = O(2)$]. These measurements suggest that there is an overall reduction in the size of the eddies that cause pressure fluctuations and, in particular, of the larger eddies. Similar results by Willmarth et.al.(1976) for [$\delta/a = O(4)$] confirm the reduction in size of the turbulent eddies, and it is suggested that these effects are related to the increased fullness of the velocity profile, and to the limited lateral extent

of that part of the axisymmetric boundary layer in which shear stresses are significant. The increased fullness of the profile requires that eddies moving at a given convection velocity will attain a given mean speed closer to the wall, requiring a reduction in the size of the eddy. The lateral limitation results in a lateral shearing action by the free stream on the larger eddies when they grow or move laterally.

The effects of increasing δ/a, as observed by Willmarth et.al.(1976), include an increase in the fraction of the cylinder circumference (to approximately one half) over which pressure fluctuations are correlated, suggesting that when δ/a is large, the structure and evolution of the larger eddies, after formation, become independent of the presence of the wall. The results of Panton et.al.(1980) for wall-pressure fluctuations in an axisymmetric boundary layer with small δ/a (0.05) on the fuselage of a sailplane show no transverse curvature effects.

The mechanism by which the small surface area of a slender cylinder may sustain the large volume of turbulent boundary layer has been examined by Luxton et al.(1984) and Bull et al.(1988), in the $25 < \delta/a < 50$ regime. These authors suggest that large scale motions in the outer boundary layer appear to strip sections of low speed fluid from the inner layer, causing the continuous regeneration of the inner layer and hence generating sufficient vorticity and turbulent energy to sustain the thick boundary layer. This mechanism is proposed as the dominant form of turbulence generation in thick turbulent boundary layers on cylinders in axial and near-axial flow. Such a dominance may form the basis for the volume of turbulence per unit surface area in an axisymmetric boundary layer being greater than that in flat-plate boundary layers by a factor of the order of $\delta/2a$, which factor can easily be as high as 20.

A comprehensive study by Lueptow and Haritonidis (1987) in the [$\delta/a = O(8)$] regime, which involved the measurement of mean and fluctuating velocity components, VITA and *uv*-quadrant analysis, and flow visualisation in water [$\delta/a = O(20)$], produced two major results: first, the detection of a burst cycle near the wall similar in nature to that in a flat-plate layer, and, second, the observation of large scale structures moving from the outer region on one side of the cylinder to the opposite side with little interference from the cylinder itself. Although the observed burst cycle appears similar to the flat-plate mechanism, its interaction with the outer flow is different, resulting in a larger friction coefficient and thus implying a more effective method of converting mean flow energy into turbulence energy.

It is suggested by Lueptow and Haritonidis (1987) that the observed cross-flows are related to the more effective mechanism, and that as δ/a becomes even larger, the mixing is largely a result of the inertia of the larger eddies, and thus the mixing length is effectively constant throughout the outer layer. This supports the use of the constant-eddy-viscosity closure used by Lueptow et.al.(1985) and Lueptow and Leehey (1986)in their analytical description of the axisymmetric turbulent boundary layer.

In summarising previous results, Lueptow (1988,1990) concludes that as δ/a becomes large, the flow behaves as a hybrid of an axisymmetric wake and a boundary layer, with the cylinder wall acting to convert mean-flow energy into turbulence energy, thus continuously regenerating the wake by the production of vorticity and turbulence along the wake centerline. Flow visualisation of the near-wall region of turbulent axisymmetric boundary layers [$\delta/a = O(16)$] by Lueptow and Jackson (1991) reveals a similar streaky structure to that found by Kline et.al.(1967) in planar

boundary layers leading them to conclude that the axisymmetric burst cycle and the planar mechanism in the near-wall region are similar. These findings are supported by a numerical investigation by Neves et.al.(1991) for $\delta/a = 0$, 5, and 11, with the addition of an estimation of a constant mean spacing of the observed streaks of approximately 90 - 100 wall units relative to the cylinder perimeter of 137 wall units [$\delta/a = 11$].

Measurements by Wietrzak and Lueptow (1994) of the fluctuating wall shear stress and velocity components for $\delta/a = 5.7$ also demonstrated the existence of a planar-type burst cycle as the dominant mechanism in the axisymmetric layer. However their measurements also indicate the existence of smaller structures occurring at higher frequencies. These structures are possibly related to fluid from the outer layer washing over the cylinder. Wall pressure measurements by Snarski and Lueptow (1995) for $\delta/a = 5$ also confirm the presence of a burst mechanism with only minor variations from the planar mechanism. Further investigations of the wall pressure by Bokde et.al.(1999) for $\delta/a = 4.81$, and of both wall pressure and shear stress by Nepomuceno and Lueptow (1997) for $\delta/a = 5$ also show little variation from the planar case.

The current issues in axisymmetric turbulent boundary layer investigations are comparable to those in flat plate layers, namely the origin and evolution of vortex structures, and the interaction between the inner and outer layers, with the addition of the effect of δ/a on these mechanisms. The preceding research suggests that for $\delta/a < 20$, the axisymmetric turbulence mechanisms are similar to the planar mechanisms. The observations of Luxton et.al.(1984) and Bull et.al.(1988) for $\delta/a > 20$ allow the possibility that the planar mechanism is either highly modified, or becomes overshadowed by a separate mechanism related to turbulent cross flows at large δ/a.

2.3 Boundary Layers on Cylinders at Angles of Yaw.

Previous examinations of the boundary layer on cylinders yawed to the flow have been concerned primarily with cylinders at large angles of yaw ($\beta > 30°$) and of moderate slenderness ratio ($l/d < 50$). They have described the effects of yaw angle relative to the case of a cylinder normal to the flow.

The effect of cylinder yaw on the mean properties of the boundary layer has been examined analytically for large angles of yaw for the laminar case by Sears (1948), whose initial results were applied successfully and extended by Cooke (1950) for a cylindrical wedge, by Moore (1956) for a swept aircraft wing, and by Chiu and Lienhard (1967) for the boundary layer separation and vortex shedding behaviour of a circular cylinder. Cebeci (1974) has extended the analytical analysis of the mean properties to include turbulent flows, by the use of an eddy-viscosity formulation for the closure assumption in the solution of the equations of motion, and has confirmed by experiment the theoretical results for swept wings and plates at large angles of yaw.

The effect of yaw angle on laminar flow stability and on laminar-turbulent transition, relative to the process for cylinders normal to the flow, has been examined by Poll (1985), Malik and Poll (1985), and Takagi and Itoh (1994) for large yaw angles. Allen and Riley (1994) have explored numerically the boundary layer on a yawed body of revolution at large β using both a finite difference method and a spectral method with particular regard to determining a description of the flow separation.

The more complex case of the effect of small angles of yaw on a long slender cylinder [l/d = $O(200)$] in near-axial flow ($\beta < 10°$), relative to the axial flow case of a thick axisymmetric turbulent boundary layer, has been investigated by Willmarth et.al.(1977) for both mean boundary-layer properties and turbulence-generating mechanisms. The iso-velocity contours generated from measurements of the boundary-layer velocity profile at various azimuthal locations around the cylinder perimeter indicate that even small angles of yaw ($\beta < 1°$) produce marked asymmetry of the boundary layer. This asymmetry has been verified by Bucker and Lueptow (1998) for very small yaw angles of $\beta \leq 0.55°$ where the boundary layer thickness was found to increase non-linearly with yaw angle. This implies that the flow properties within the boundary layer in axial or near-axial flow may be highly dependent upon any localised yaw introduced by either disturbances in the free stream or non-alignment of the cylinder axis.

The results of Willmarth et.al.'s (1977) fluctuating wall pressure measurements were largely inconclusive as a means of determining yaw effects on the mechanisms of turbulence production in thick turbulent boundary layers. These effects are still not understood fully. The possibility of a relationship between such mechanisms for the production of turbulence and vorticity and the initiation of vortex shedding at very small angles of yaw has yet to be investigated.

2.4 Vortex Shedding from Cylinders Normal to the Flow.

Vortex shedding from circular cylinders with their axes normal to a flow (i.e. at yaw angles of $\beta=90°$ in the terminology used here) has received considerable attention in the past in its own right, and results for this case have also been used extensively as a basis for correlating data relating to cylinders at other inclinations to the flow.

Detailed quantitative knowledge of regular vortex shedding from circular cylinders normal to a flow stems from the pioneering hot-wire investigations of Kovasznay (1949) and Roshko (1954). These early works identified the various vortex-shedding regimes and the Reynolds number ranges in which they occur.

Roshko's investigations for $40 < Re_d < 10{,}000$ established that periodic vortex shedding occurs over two distinct subranges: the 'stable range' from $Re_d = 40$ to 150, in which regular vortex streets are formed and no turbulent motion is detected, and the 'irregular range' for $Re_d > 300$ in which turbulent velocity fluctuations in the wake accompany the periodic formation of vortices. These two ranges are separated by a 'transition range' from $Re_d = 150$ to 300, in which turbulence is initiated by laminar-turbulent transition in the free shear layers which spring from the separation points on the cylinder. Empirical relationships between the frequency parameter $F = fd^2/\nu$ and Re_d were determined by Roshko to be as follows:

$$50 < Re_d < 150 \qquad F = 0.212\, Re_d - 4.5 \qquad [2.1]$$

$$300 < Re_d < 2000 \qquad F = 0.212\, Re_d - 2.7 \qquad [2.2]$$

with a maximum error of less than 1 percent.

An analytical solution for the velocity field of the viscous vortex street generated by a circular cylinder in the Reynolds number range $50 < Re_d < 125$, is presented by Schaefer and Eskinazi (1959). The analytical description of the flow divides the vortex street into three areas of behaviour: the 'formation', 'stable' and 'unstable' regions, and this interpretation is supported by the authors' experiments.

In the formation region immediately behind the cylinder where the vortex street develops, some partial cancellation of positive and negative vorticity (from opposite sides of the cylinder) occurs. In combination with diffusion, this results in the vortices subsequently formed having a somewhat lower circulation than that shed directly from either side of the cylinder. In the stable region the vortex street is fully developed and the vortices display a periodic regularity. Further downstream is the unstable region, in which the flow exhibits irregular behaviour followed by eventual transition to turbulence. At values of Re_d greater than approximately 125, the stable region of the vortex street is no longer apparent.

The geometrical arrangement of the vortices in the stable wake is given by von Karman's theory; however experimental results demonstrate variations from this geometry. Von Karman's theory also fails to determine the vortex shedding frequency. The mechanism by which the frequency is determined was examined by Nishioka and Sato (1978), who proposed the use of stability theory of shear flows to predict the growth rate of small-amplitude fluctuations where the frequency of the fluctuations with the highest growth rate should determine the vortex shedding frequency. In the stable

range below Reynolds numbers of $Re_d = 70$, the shedding frequency is found to be determined by the linear growth of small fluctuations. Non-linear effects become dominant at higher Reynolds numbers, but the Strouhal number remains predictable up to Reynolds numbers of $Re_d = 120$.

Discontinuities in the F - Re_d relationship, and variations from Equation [2.1] were first published by Tritton (1959) for a discontinuity in the Reynolds number region $80 < Re_d < 105$. Tritton suggested that Roshko's Equation [2.1] be replaced by two equations of the form:

$$F = a + b\,Re_d + c\,Re_d^2 \qquad [2.3]$$

with a, b and c taking the values

	a	b	c
$50 < Re_d < 105$	-2.1 ± 0.3	0.144 ± 0.010	0.00041 ± 0.00010
$80 < Re_d < 150$	-6.7 ± 0.2	0.224 ± 0.006	0 ($\lvert c \rvert < 0.00025$).

He also suggested that the frequency in the transition range $80 < Re_d < 105$ be determined by either one or the other of the above relationships and not by some combination of the two. The existence or otherwise of this discontinuity provoked extensive debate despite its verification in repeated testing by Tritton (1971).

Additional support for Tritton's discontinuity was produced by Friehe (1980) in a series of experiments using three different flow facilities and a range of cylinder l/d ratios. These experiments showed a transition in the Reynolds number range $70 < Re_d < 110$. The validity of this transition as a general principle, independent of the

peculiarities of particular experimental arrangements, is discussed at the conclusion of this section in conjunction with the conclusions drawn from the following paragraphs.

The transition to turbulence in the wake of a circular cylinder was examined by Bloor (1964) for Reynolds numbers from Re_d = 200 to 50,000 , where the region 200 < Re_d < 400 was identified as Roshko's (1954) 'transition region' below which no turbulent motion is generated. Bloor found that, within the transition region, the position of the transition to turbulence moves towards the cylinder as the Reynolds number is increased, and that the corresponding mode of transition is dominated by large scale three-dimensionalities in the flow.

At Re_d = 400, the vortices are turbulent on formation, and the location of the transition is stable as Reynolds number is increased to 1,300 ; at higher Re_d the region of laminar flow begins to decrease, the region of transition almost reaching the shoulder of the cylinder at Re_d = 50,000. The mode of transition above Re_d = 400 is dominated by two-dimensional instability; this leads to the production of Tollmien-Schlichting waves and eventually turbulence through small-scale three-dimensionalities.

The three-dimensional nature of the wake was investigated for stable, transitional and turbulent vortices by Gerrard (1966a) using an array of hot-wire probes along the cylinder length at Reynolds numbers of 85, 235 and 20,000. For the stable vortex street Gerrard demonstrated that the shed vortices occur in straight lines inclined to the cylinder axis, and suggested that modulations detected in the vortex shedding frequency result from the wake flapping somewhat like a flag in the wind. In the transitional region, Gerrard found the dominant three-dimensional feature to be the

simultaneous occurrence of laminar and turbulent vortices at different positions along the cylinder length. He suggested that the vortex lines were now both wavy and inclined. The turbulent vortices were found to form in straight lines parallel to the cylinder axis, with small random variations in inclination occurring with time.

Gerrard (1966b) further examined the formation region of vortices for Reynolds numbers greater than $Re_d = 400$, and proposed the simultaneous existence of two characteristic lengths, the length of the formation region, and the width of diffusion of the shear layers. Because the length of the formation region decreases and the diffusion width increases as the Reynolds number is increased, the resulting Strouhal number remains approximately constant at $St = 0.21$ for Reynolds numbers $Re_d > 400$. At the time, Gerrard was not able to make reliable quantitative measurements of the vortex shedding frequency to support his proposed underlying processes. Later Gerrard (1978) conducted a comprehensive flow visualisation study of the wakes of cylinders in water flow for Reynolds numbers from $Re_d = 0$ to 2,000, using dye washed from the rear surface of cylinders in a towing tank.

Gerrard's visual study outlined a series of flow regimes within the Reynolds number range studied. The regimes were not separated by abrupt transitions, but were observed to merge gradually into one another; and at the transition Reynolds number the flow was found to change with time between regimes. These flow regimes are summarised by Gerrard as follows:

$0 < Re_d < 34$ Steady flow; standing eddies.

$34 < Re_d < 70$ Wavy wake, no accumulation of dye into vortices.

$55 < Re_d < 100$ Vortex street wake; remnants of the standing eddies still present; diffusion of vorticity important.

$100 < Re_d < 140$ Increased efficiency of convective mass transfer behind the body; an accelerating phase of vortex motion present up to $Re_d = 500$.

$140 < Re_d < 500$ Fingers of dye moving back towards the body from the wake; vortex strength irregular; more nearly two-dimensional flow; transition to turbulent vortex cores downstream.

$250 < Re_d < 400$ Transition to high Re_d type of vortex shedding.

$350 < Re_d < 2000+$ Transition waves in the separated layers and transition to turbulence in the vortex cores on formation.

Gerrard qualifies these results with an observation on the sensitivity of the flow to disturbances, in particular to the end conditions of the cylinder. He suggests that any conclusions drawn from such experiments must be related to the experimental arrangement involved. This is now recognised as one of the features of real turbulent wakes shed from finite aspect ratio cylinders and also from large aspect ratio cylinders.

The three-dimensional effects caused by variations in flow velocity along the cylinder length were examined by Gaster (1969 and 1971) who suggested that the

vortex shedding frequency is determined by the local conditions. Where the variations along a cylinder are slight, Gaster determined that the vortices are shed in cells of constant frequency, with abrupt changes between adjoining cells. Such cell patterns had previously been observed by Humphreys (1960) at the much higher Reynolds numbers associated with the laminar-turbulent transition in the range Re_d = 40,000 to 600,000.

The positions of the cell boundaries were shown by Gaster to vary with time along the cylinder length, unless fixed in place by end-plates fitted to the cylinder. Gaster suggested that Tritton's results (1959) were caused by the presence of such a shear flow, and that the discontinuity observed at Re_d = 90 is not a general flow phenomenon, but rather the effect of such cell boundaries moving along the cylinder, causing the shedding frequency to jump between different constant values. Further evidence that vortices form in discrete cells, and are thus not correlated along the entire cylinder span even in a uniform flow, is provided in a survey of the correlation lengths of vortices along the cylinder axis by Graham (1966). This indicates that the correlation length decreases throughout the stable shedding region, and then remains constant throughout the irregular shedding region; however the measured correlation length appears to be extremely dependent on the cylinder end conditions, vibration, noise and flow irregularities.

Further work on the effect of shear flows on vortex shedding by Maul and Young (1973) and Sobey and Mitchell (1977) supports Gaster's proposals on the formation of cells. An analytical model of cell formation for a cylinder in a non-uniform flow has been formulated by Noack et.al.(1991). This model predicts the location of the cells, their frequencies, amplitudes of oscillation along the span, and the

local shedding angle. It is shown to agree in general qualitative features with experimentally observed cell properties.

The effect of end-plates on a vortex wake was investigated by Stansby (1974) by measuring the variation of cylinder base pressure along the span. Stansby demonstrated that end-plates could be used to produce a two-dimensional flow from an initial flow with considerable spanwise variation. A more detailed examination by Graham (1969) demonstrated that for aspect ratios (of the cylinder between the plates) less than four, the flow becomes two-dimensional, and that at larger aspect ratios there is little or no spanwise correlation between the vortex streets at positions a large distance apart, suggesting that there are limitations on the spanwise influence of end-plates. These limitations have been examined by Szepessy and Bearman (1992) for aspect ratios in the range ($l/d = 0.25 - 12$), and ($Re_d = 8{,}000 - 140{,}000$), by measurements of spanwise correlation. The effect of changing aspect ratio is found to be Reynolds-number dependent, having a weak effect at low Re_d and a much stronger effect at higher Re_d. Thus two-dimensional flow is only produced by end-plates for small cylinder aspect ratios at high Reynolds number.

A review of vortex shedding phenomena by Berger and Wille (1972) raised the suggestion that variations in end conditions between different experimental arrangements may be the basis of conflicting results, and that such variations may become apparent in the observed inclination to the cylinder of the lines of shed vortices. Strouhal numbers for $40 < Re_d < 160$ were also found to vary for different levels of free stream turbulence between different facilities. A later review of vortex shedding, by Bearman and Graham (1980), added further support to the influence of

free stream turbulence on vortex shedding behaviour. These variations raise a problem in relation to the use of Roshko's Equations [2.1] and [2.2] as a means of measuring flow speed. However, investigations by Kohan and Schwarz (1973) suggest that once a vortex-generating cylinder is calibrated for a particular facility, it remains an extremely accurate tool for determining flow speed.

Variations in end conditions were examined by Slaouti and Gerrard (1981) by visualisation of water flow over a vertical cylinder in a towing tank for Reynolds numbers in the range Re_d = 60 to 200. The effect of end conditions resulting from a contaminated or clean water surface, from end plates and free ends, and from a gap between the surface and a cylinder free end were examined.

All of these end conditions were found to dominate the flow near the cylinder ends, and thereby to influence strongly the complete wake structure. A further study of the influence of end plates and free ends on vortex shedding behaviour, conducted by Gerich and Eckelmann (1982), showed that frequency variations in the order of 10 - 15% could be produced up to 15 diameters from the cylinder ends by varying end conditions.

The large influence of end conditions is supported by an examination of von Karman's theory by Sirovich (1985), and experimental investigations by Sreenivasan (1985), which indicate that the Strouhal-number / Reynolds-number relationship may be partially indeterminate, with the outcome for particular regions of Re_d being dependent on the initial or boundary conditions.

Sreenivasan's studies over the Reynolds number range of 30 to 10,000 indicate that the "initial stages of transition to turbulence are characterised by narrow windows of chaos interspersed between regions of order". A further examination of such 'ordered' and 'chaotic' vortex streets, undertaken by Van Atta and Gharib (1987), suggests that the mechanism by which the regions of chaos observed by Sreenivasan occur is by aeroelastic coupling of the vortex wake with cylinder vibration modes.

Williamson (1988) has shown that the extreme sensitivity to end conditions allows spans of up to 240 diameters to be influenced by end effects. By measuring the shedding angle α, and transforming the measured Strouhal number St_α to $St = St_\alpha/\cos \alpha$, Williamson has produced a single continuous Strouhal-number / Reynolds-number curve for the regime of regular shedding. This correlation is based on the assumption that, in the absence of end effects, shedding takes place parallel to the cylinder axis. However further analysis by Williamson (1994) suggests that the absence of end effects does not necessarily result in parallel shedding. From an analysis of data for cylinders of large aspect ratio ($l/d > 100$), Norberg (1994) found that the Strouhal number becomes independent of aspect ratio at large l/d, suggesting a spanwise limitation to the influence of end effects.

Further work on the manipulation of the end conditions to produce parallel shedding, by Eisenlohr and Eckelmann (1989), demonstrates that a small step change in the cylinder diameter at both ends can decouple the wake flow from the disturbances deriving from end conditions. These results suggest that Graham's (1969) finding of the limited spanwise effect of endplates was the result of using endplates to produce a two-dimensional flow from a free stream with some three-dimensional characteristic (such

as a transverse velocity gradient) rather than an independent effect of the end conditions. A Strouhal-number/Reynolds-number relationship for parallel shedding has been proposed by Fey et.al.(1998), based on their experimental data for parallel shedding achieved by the use of either a step change in cylinder diameter or end plates to control the end effects. Investigations by Konig et.al.(1990) indicate that the Strouhal-number/Reynolds-number relationship is also influenced by the level of free stream turbulence, particularly the exact location of the discontinuities in the relationship.

An alternative method of decoupling the wake flow from the cylinder end effects is proposed by Hammache and Gharib (1989) in which two control cylinders of larger diameter, placed upstream of the test cylinder and normal to both the flow and the test cylinder, are used to impose a symmetric pressure boundary condition at the two ends of the cylinder. Further analysis by Hammache and Gharib (1991) of the effects of non-symmetric pressure distribution along the span, indicates that the resulting oblique shedding is a function of the induced spanwise flow in the base region of the cylinder, and that a simple flow model based on the ratio of the streamwise to the spanwise vorticity components allows the shedding angle to be predicted within two degrees.

An analytical model based on a Ginzburg-Landau equation formulated by Albarede and Monkewitz (1992) and Albarede and Provansal (1995) indicates that symmetric end pressures may not produce parallel shedding but rather a symmetric "chevron" pattern formed by oblique shedding growing inwards from both ends, and that the oblique shedding observed for non-symmetric end pressures is a result of the

inward growing "half-chevron" with the larger shedding angle spreading across the entire cylinder span.

Investigations by Anderson and Szewczyk (1997) and Ozono (1999) of the effects of splitter plates in the near wake have shown that nominally two-dimensional flows exhibit significant three-dimensional behaviour, which may be modified to appear two-dimensional by manipulation of the cylinder radius (taper) or local free stream velocity (shear layer flow), and by the use of splitter plates. The results of manipulation of the shedding angle by the use of inclined end plates, obtained by Prasad and Williamson (1997), indicate that the discontinuity in the Strouhal-number variation in the vicinity of $Re_d = 250$ does represent the infinite aspect ratio case, and is not due to end conditions modifying the infinite aspect ratio behaviour. These results suggest that, although particular experimental arrangements may be used to produce vortex wakes which appear two-dimensional, the wakes are in fact always three dimensional.

A review of developments in understanding cylinder wakes undertaken by Williamson (1996) has emphasised the importance of the three-dimensional aspects of nominally two-dimensional flows. Williamson also stresses the need to distinguish between the "intrinsic" three-dimensional aspects of the flow arising from natural instabilities, and the "extrinsic" three-dimensional aspects resulting from end conditions and other external effects.

The investigations of vortex shedding from circular cylinders normal to the flow provide a base of knowledge in flow mechanisms and experimental techniques which is

applicable to the more complex problem of vortex shedding from yawed cylinders. In particular these investigations have revealed major sources of uncontrolled experimental variation such as cylinder end effects, free stream shear flows and turbulence levels, and aeroelastic and other vibrations.

For cylinders normal to the flow, the effects of cylinder end conditions and free-stream shear flows may be considered to have been negated in experimental arrangements where either symmetric or parallel vortex shedding is observed. This principle may not be extended to the case of yawed cylinders where the presence of both normal and axial components of vorticity results in a net vorticity vector which may produce lines of shed vortices which are inclined to the cylinder axis. However, the success of Hammache and Gharib (1991) in determining shedding angles for cylinders normal to a shear flow by the calculation of spanwise and streamwise vorticity components suggests that a similar method may be applicable to yawed cylinders in a uniform flow. A numerical simulation of the vortex wake by Jordan and Ragab (1998), using the large eddy simulation method, has reliably reproduced previous experimental results for the velocity in the near wake. This raises the possibility of reliable numerical simulation of the yawed cylinder wake in the future.

2.5 Vortex Shedding from Cylinders at Angles of Yaw.

Previous investigations of vortex shedding from yawed circular cylinders have concentrated on the effect of deviations in cylinder alignment from the normal flow case. Such studies do not extend to small angles of yaw from the axial direction (i.e. small β). Their primary concern is with the range $90° > \beta > 15°$, with an emphasis on describing the vortex shedding process as a variation from the normal cylinder case. Initial experiments on vortex shedding from cylinders at small yaw angles were conducted in the Department of Mechanical Engineering in the University of Adelaide by final-year undergraduate students Azadegan (1987) and Circelli (1988). In both cases the results indicated the presence of vortex shedding when β is small.

Hot-wire studies by Hanson (1966), of vortex shedding from cylinders at yaw angles from $\beta = 90°$ to 18°, formed the basis for the application of the so-called 'independence principle' to vortex shedding from yawed cylinders. The 'independence principle' asserts that the shedding frequency is determined solely by the component of flow velocity normal to the cylinder axis, and is independent of the axial velocity component. Hanson's investigations are within Roshko's (1954) 'stable' range of Reynolds number (from $Re_d = 40$ to 150), in which the vortex shedding behaviour of a normal cylinder is described by Roshko's Equation [2.1]. Hanson uses the independence principle to reformulate Equation [2.1] for yawed cylinders in the stable shedding range as:

$$F = 0.212\ Re_n - 4.5 \qquad [2.4]$$

where $Re_n = Re_d \sin \beta$.

Hanson's results for angles β of 90, 63, 45, 34, 22 and 18 degrees show good agreement with Equation [2.4] except for the data at $\beta = 18°$. In addition, Hanson found the critical Reynolds number (at which vortex shedding first occurs), based on the normal component of the flow, to be approximately constant for $\beta > 40°$. From these observations Hanson concludes that Equation [2.4] is a useful measure of the effect of cylinder yaw on the frequency of vortex shedding. Support for this conclusion comes from the experiments of Surrey and Surrey (1967) who examined cylinders at similarly large yaw angles, but at much higher Reynolds numbers (4,000 - 65,000). With decreasing yaw angle, their Strouhal number based on the normal velocity component remains approximately constant, and correspondingly the energy of the shed vortices decreases in significance, becoming negligible in comparison with the general wake turbulence at $\beta < 50°$.

An analytical study of fluid flow over yawed cylinders was undertaken by Chiu and Lienhard (1967). Based on their theoretical investigation of boundary-layer formation and separation, they found the vortex-shedding behaviour to be determined solely by the cross-flow in the region of large β and high Re_d. These conclusions were supported by experiments conducted by Chiu (1966) in the Reynolds number range $3{,}900 < Re_d < 21{,}200$ for angles of yaw in the range $30° < \beta < 90°$. Chiu and Lienhard's investigation of the region of validity of Equation [2.4] suggests that large deviations from the independence principle can be expected for $Re_d < 300$ where the wake thickness begins to vary with Reynolds number. Van Atta (1968), who initially intended to examine the anomaly in Hanson's (1966) results for $\beta = 18°$, showed that many of Hanson's data were affected by locking of the vortex-shedding frequency to the cylinder's natural vibrational frequency.

A further investigation of such aeroelastic coupling, between structural vibrations and fluid forces, was conducted by King (1977) for yawed cylinders in the range $45° < \beta < 90°$. King observed such coupling for the wide range of Reynolds numbers from Re_d = 2,000 to 20,000.

Van Atta (1968) examined the "lock-in" process by using a phonograph cartridge to detect cylinder vibrations, while varying the natural frequency by adjusting the cylinder tension. These investigations demonstrated that lock-in tends to occur by a lowering of the shedding frequency to that of a natural vibration mode near the frequency given by Equation [2.4]. Van Atta suggests that this behaviour indicates that the cross-flow alone excites cylinder vibrations, and that this effect explains why Hanson's frequency observations can be reduced to Equation [2.4].

Van Atta (1968) proceeded to investigate vortex shedding from non-vibrating cylinders over the Reynolds number range $50 < Re_d < 600$ at angles of yaw from $\beta = 90°$ to 14°. For these flow conditions, Van Atta obtained results at constant normal Reynolds numbers of Re_n = 50, 80 and 150 which indicate that the independence principle is invalid for angles of yaw $\beta < 60°$. This suggests that the components of flow are not independent, but that at large angles of yaw (large β) the vortex shedding behaviour is very heavily dominated by the normal flow component. Experiments were made at higher Reynolds numbers by Smith et al. (1972). While their measured vortex-shedding frequencies are consistent the independence principle in the range $1,000 < Re_d < 10,000$ for $\beta = 90°$ to 30°, their detailed examination of wake properties shows that the cylinder base pressure and the position of the transition to turbulence do not obey the independence principle.

The Reynolds number range between van Atta's (1968) results ($Re_d < 600$), and Smith's (1972) results ($Re_d > 1000$) was examined by Knaus et al. (1976) for a yaw angle of $\beta = 50°$. Their results show that for $390 < Re_d < 1560$ the vortex shedding frequency is 8 - 10% higher than that predicted by the independence principle, with a trend toward the predicted values at increasing Re_d.

A detailed study by Ramberg (1983), of both stationary and vibrating yawed cylinders in the Reynolds number range $Re_d = 150$ to 1,100 , for angles of yaw $\beta = 90°$ to 30°, examined the effect of end conditions on the vortex shedding process. Ramberg examined the vortex shedding angle α by using a strobe light to illuminate aerosol particles in an air flow. These observations indicate that the cylinder end conditions can dominate the wake behaviour for spans of up to 100 diameters. Ramberg observed that in the absence of end effects shedding occurs with the vortex lines inclined to the cylinder axis; he supports this observation with physical arguments that such inclined shedding results from the presence of a component of vorticity associated with the axial flow component, which causes the net vorticity vector to be inclined to the cylinder axis. Ramberg's observations of vibrating yawed cylinders indicate that shedding parallel to the cylinder axis occurs when the vortex shedding frequency locks-in to the cylinder vibrational frequency.

Ramberg's observations and arguments for inclined vortex shedding suggest that the independence principle has no validity, except in specific cases, such as that of vibrating cylinders. His observation that the shedding frequency may vary with changes in the shedding angle, caused by non-ideal end conditions, suggests that previous results may have also been subject to such variation.

In the investigation by Shirakashi et al.(1986) for Re_d = 800 to 55,000 and angles of yaw from β = 45° to 90°, flow visualisation by smoke streaks showed that the flow over a yawed cylinder is highly three-dimensional in nature. Only when the secondary flow behind the cylinder is suppressed (by plates in the cylinder wake) does the shedding frequency become equal to that for a cylinder subject to only the normal velocity component of the flow. From these observations, it was concluded that data correlations resulting from the application of the independence principle are largely fortuitous.

Computational analysis by Kawamura and Hayashi (1994) of the wake of a yawed cylinder at β = 60°, Re_d = 2,000 for cylinders of both finite and infinite aspect ratio ($l/d < 15$ and $l/d = \infty$) indicate a weak three-dimensional spanwise structure for the infinite cylinder accompanied by a secondary flow propagating downstream along the cylinder axis, and a strong three-dimensional structure for the finite aspect ratio cylinders. An experimental analysis of the wake by Hayashi and Kawamura (1995) (for β = 60°, 45° and 30°; Re_d = 15,000; l/d = 20) identified a quasi-two-dimensional region of the wake (such that the flow has a similar pattern in any section parallel to the free stream) along the receding half of the span.

These results raise the possibility that for cylinders of large aspect ratio ($l/d > 100$), a quasi-two-dimensional flow may be established over the majority of the span where the secondary flow propagating along the cylinder axis has become fully developed. As β is decreased this secondary flow is expected to increase in strength and thus require a greater length to develop, or, alternatively, to continue to develop without ever establishing the fully developed state required for quasi-two-dimensional flow.

From the foregoing it is clear that interaction between the axial and normal components of the flow increases as the yaw angle β is decreased (i.e. as the cylinder axis approaches alignment with the flow direction) and as the Reynolds number Re_d is decreased. The independence principle has been shown to be invalid for a stationary yawed cylinder of infinite length, although it gives a good prediction of the vortex shedding frequency when the cross-flow is heavily dominant. In the absence of the independence principle the relationship of the Strouhal number to the Reynolds number and the yaw angle has yet to be determined for the three-dimensional flow.

As for the normal cylinder case, the flow is found to be strongly influenced by the cylinder end conditions, an influence that is best detected by observation of the vortex shedding angle. In the absence of end effects this shedding angle for yawed cylinders has yet to be determined as a function of Reynolds number and yaw angle, although physical arguments and observations suggest that the vortex lines occur between $90°$ and $\beta°$ to the flow direction.

2.6 Literature Review: Key Conclusions.

1. The overall mechanism for the production of turbulence in the planar boundary layer is not yet fully understood; however, the dominant mechanisms may be described by the burst cycle.

2. For cylinders of small transverse curvature ($\delta/a < 5$), the turbulence mechanisms within the axisymmetric boundary layer appear to be similar to those of the planar boundary layer.

3. For cylinders of moderate transverse curvature ($5 < \delta/a < 20$), a burst cycle similar to the planar mechanism appears with the addition of large turbulent cross-flows.

4. For cylinders of large transverse curvature ($\delta/a > 20$), the thick axisymmetric boundary layer takes on a wake-like character, and the relative importance of the burst cycle and of the turbulent cross flows in the production of turbulence is not yet fully understood.

5. The ratio of the volume of a boundary layer to the surface area supporting it is greater for a slender cylinder in axial flow than for a flat plate by a factor of the order of $\delta/2a$, which may be as high as 20 or more. This observation suggests the presence of a more efficient vorticity-generation mechanism, possibly related to turbulent cross-flows, than occurs in planar boundary layers.

6. The axial boundary layer on a slender cylinder is maintained for small angles of inclination β between the cylinder axis and the flow direction. The shape of the boundary layer cross-section becomes increasingly elongated to the leeward side of the cylinder with increasing β, and shows marked asymmetry at angles of yaw as small as $\beta = 1.0°$.

7. The vortices shed from a cylinder normal to the flow may be generated with their axes either parallel to the cylinder axis or in the form of symmetric chevrons, in the absence of end effects and three-dimensional flow characteristics in the free stream.

8. For cylinders normal to the flow, the vortex-shedding frequency at constant Reynolds number will vary with changes in end-conditions, since the end-conditions affect the angle between the vortex lines and the cylinder axis. Such variations appear to be the cause of discontinuities in the Reynolds-number / Strouhal-number relationship which are not always reproducible under different experimental arrangements.

9. The independence principle, (the notion that velocity components normal and parallel to the cylinder axis produce independent effects) has been shown to give a good prediction of the vortex-shedding frequency of a yawed cylinder for large angles of yaw (i.e. close to normal flow) - but only in this case.

10. For cylinders with their axes inclined to the flow, the interaction between the axial and normal components of the flow becomes very significant as the cylinder yaw angle is decreased (approaching axial flow), and as the Reynolds number is decreased.

11. The independence principle has been shown to be invalid for a long slender (stationary) cylinder with its axis yawed to the flow direction, but the functional dependence of vortex-shedding frequency on flow parameters at small yaw angles has not previously been determined.

12. For cylinders with their axes inclined to the flow, the vortex lines are inclined to the flow at an angle greater than the cylinder yaw angle. In previous work, the relationship between the vortex angle and the yaw angle, as a function of the flow parameters, has not been established.

3. FACILITIES AND PROCEDURES

3.1 Low Speed Wind Tunnel

Experiments were conducted in the variable width, 3 metre long test section of the closed-circuit low speed wind tunnel shown in Figure [3.1]. The air speed in the test section can be continuously varied from 0 to 27 m/s, although the minimum stable speed is approximately 1 m/s. The airflow is generated by a belt-driven axial fan located between the first and second corners, powered by a variable speed electric motor mounted outside the tunnel on rubber vibration isolators.

The quality of the air flow entering the test section is maintained by a settling chamber containing a series of wire screens, followed by an octagonal to rectangular contraction with an area ratio of 4:1 upstream of the test section. The return circuit consists of a long diffuser with turning vanes at each corner. The entry to the return circuit consists of a bell-mouth inlet fitted with a wire screen to prevent the entry of foreign objects.

The air temperature within the wind tunnel is maintained constant by means of air exchange with the laboratory air, which is cooled by a large air-conditioning system, and may be regulated to within 1 degree. The air exchange is achieved by an adjustable vent in the low velocity section of the tunnel, upstream of the contraction, allowing high pressure heated air from the tunnel to be expelled, while additional cool air is introduced via the bell-mouth inlet upstream of the fan.

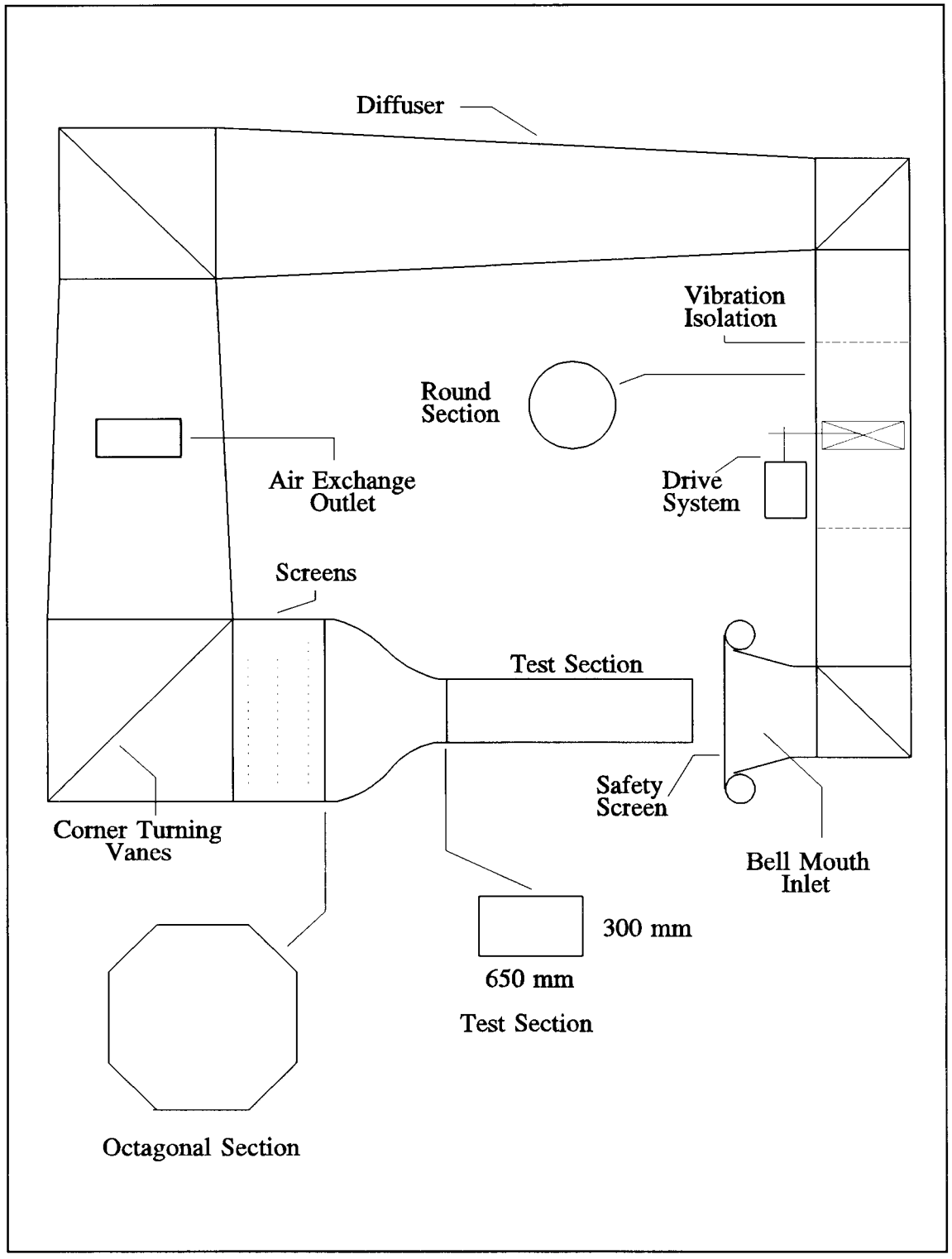

Figure 3.1 Closed-Circuit Low-Speed wind tunnel

Department of Mechanical Engineering

The University of Adelaide.

3.1.1 Variable-width test section

As the proposed experimental investigations made use of the full length of the wind tunnel test section, it was necessary to design and build a new test section capable of providing a uniform velocity distribution in the streamwise direction. This variable width test section consists of a wooden base supporting a perspex top at a height of 300 mm, and adjustable perspex side walls as shown in Figure[3.2]. The initial width at the upstream end is fixed at 650 mm to match the contraction outlet. A series of four screw jacks equally spaced along the test section length allow the section width to be varied along the section length, to a maximum of $\pm$ 200 mm at the downstream end. This allows for the establishment of a pressure gradient along the section length, or alternatively, allows for a correction to be made to remove any unwanted pressure gradient associated with boundary-layer growth on either the tunnel walls or the test cylinder, and thus to provide a uniform streamwise velocity distribution.

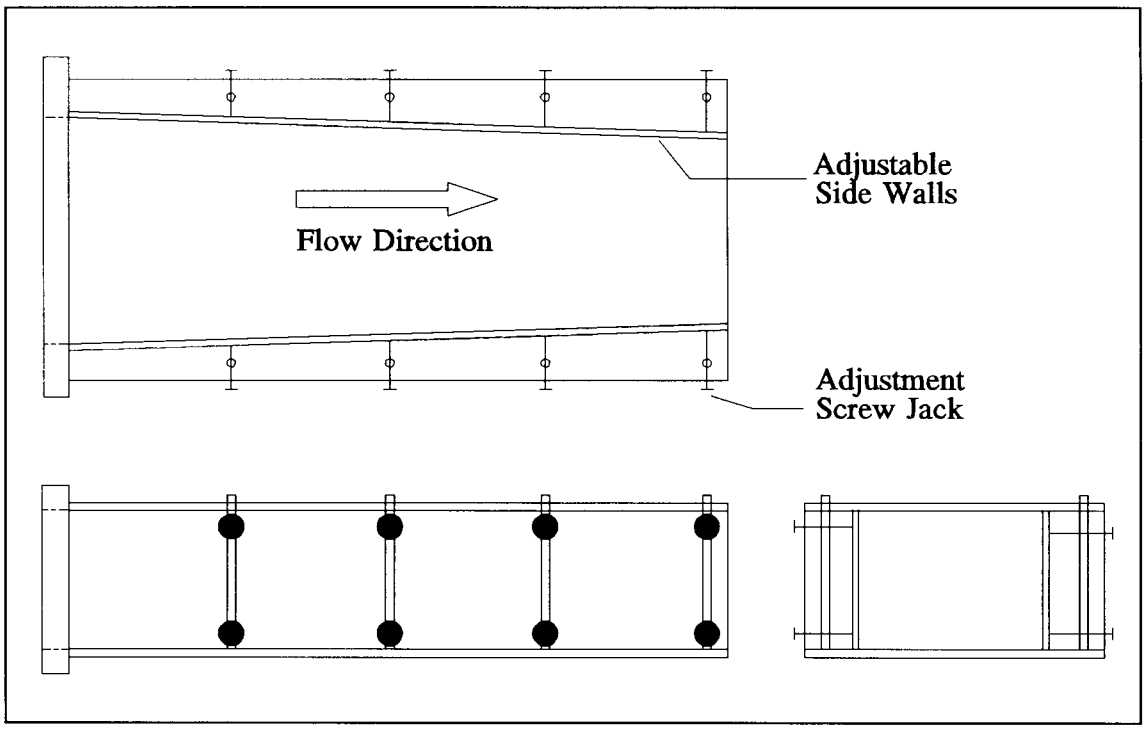

Figure 3.2 Variable-width Test Section.

3.1.2 Free-stream velocity

The mean velocity in the free stream was measured by means of a pitot-static tube, located at the same downstream location in the test section as the experiments in progress. The dynamic pressure of the air flow was measured by a null-balance manometer with a resolution of 0.01 mm and a maximum reading of 30 mm, using a manometer fluid of specific gravity 0.826. A water manometer with a resolution of 0.2 mm was used at higher velocities (above 22 m/s) where the dynamic pressure exceeded the range of the more accurate null-balance manometer.

The mean free stream velocity of the air U_1 was calculated from the measured dynamic pressure and the ambient air density as:

$$U_1 = \sqrt{(2gh\rho_m/\rho_a)} \ , \qquad [3.1]$$

where h = measured manometer head (m)

g = acceleration due to gravity (m/s^2)

ρ_m = manometer fluid density (kg/m^3)

ρ_a = ambient air density (kg/m^3) .

The ambient air density was calculated from the perfect gas equation of state using the measured air temperature and pressure as:

$$\rho_a = \left[\frac{P_a}{RT_a} \right] \ , \qquad [3.2]$$

where P_a = ambient air pressure (Pa)

T_a = ambient air temperature (K)

R = Specific Gas Constant (287 J/kg.K for air) .

Reynolds numbers were calculated using a value of absolute viscosity of air μ_a based on the ambient temperature T_a and evaluated by the Sutherland equation (Kuethe and Chow 1976):

$$\frac{\mu_a}{\mu_0} = \frac{T_0+120}{T_a+120}\left[\frac{T_a}{T_0}\right]^{\frac{3}{2}} , \qquad [3.3]$$

where the reference values of temperature and viscosity are those for standard sea level conditions:

$$T_0 = 288.16 \text{ K}$$

$$\mu_0 = 17.894 \times 10^{-6} \text{ kg/m.s} .$$

The turbulence intensity of the free-stream air flow was found to be 0.11% by hot wire anemometry using a single wire probe located on the test section centreline.

3.1.3 Streamwise velocity variation

Initial measurements were made of the streamwise velocity variation within the rectangular test section with the side-walls parallel; two null-balance manometers were used to measure the dynamic pressure at locations 500 mm and 2700 mm downstream of the entry to the test section. These measurements indicated a 5% rise in the mean velocity over this distance for flow at the downstream section at 20 m/s, increasing to a 10% rise at 4 m/s.

A traverse system was constructed to move a hot wire probe along the full length (3 metres) of the test section centreline as shown in Figure [3.3]. The probe is supported above a metal slider which is guided along the centre of the test section floor

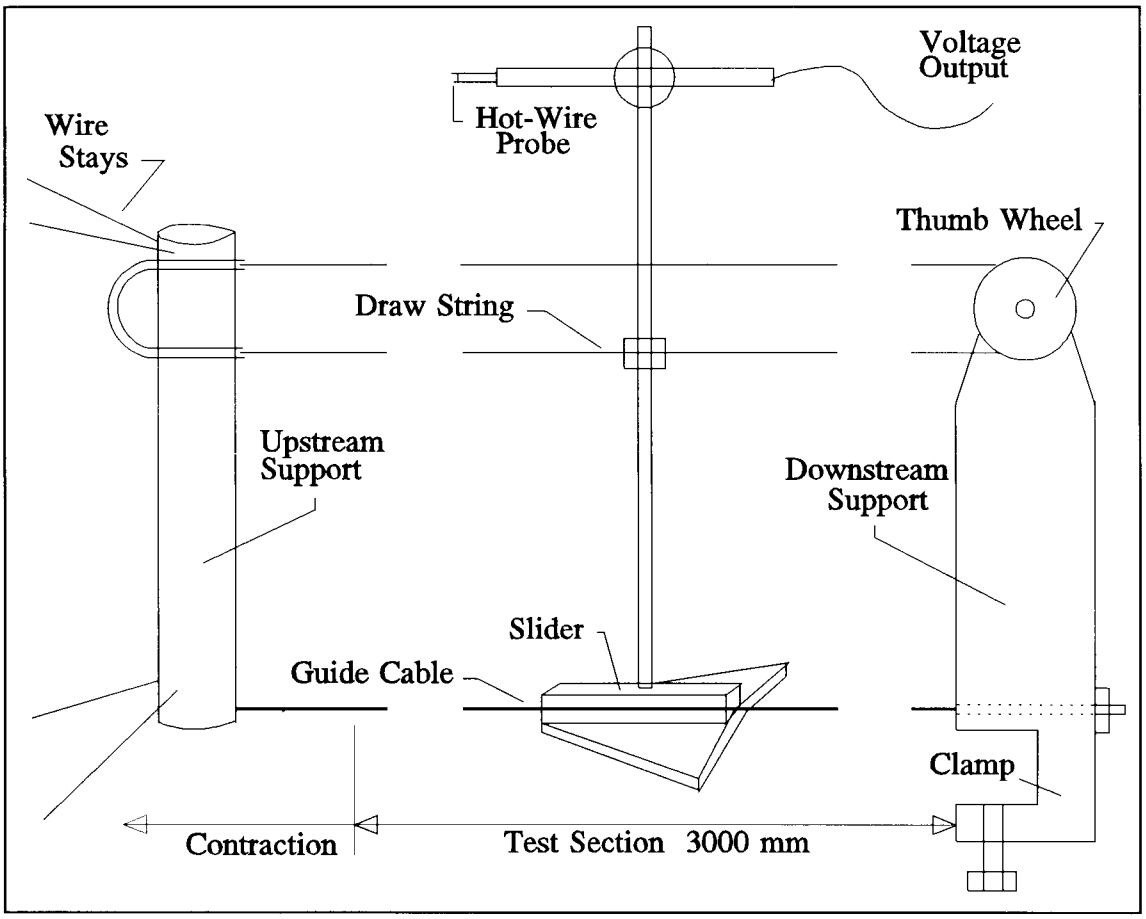

Figure 3.3 Streamwise Hot-Wire Probe Traverse.

by a steel cable attached to wire stays inside the contraction and held in tension by a clamp at the downstream end. The slider may be moved along the cable by means of a draw string and thumbwheel.

For a range of upstream velocities, the side walls were progressively moved outwards until a uniform velocity was achieved along the section length. The final side wall position at each of the adjustment points was recorded for each mean flow velocity, Figure [3.4]. All subsequent experiments were conducted with the side walls adjusted in accord with these data to provide uniform streamwise velocity.

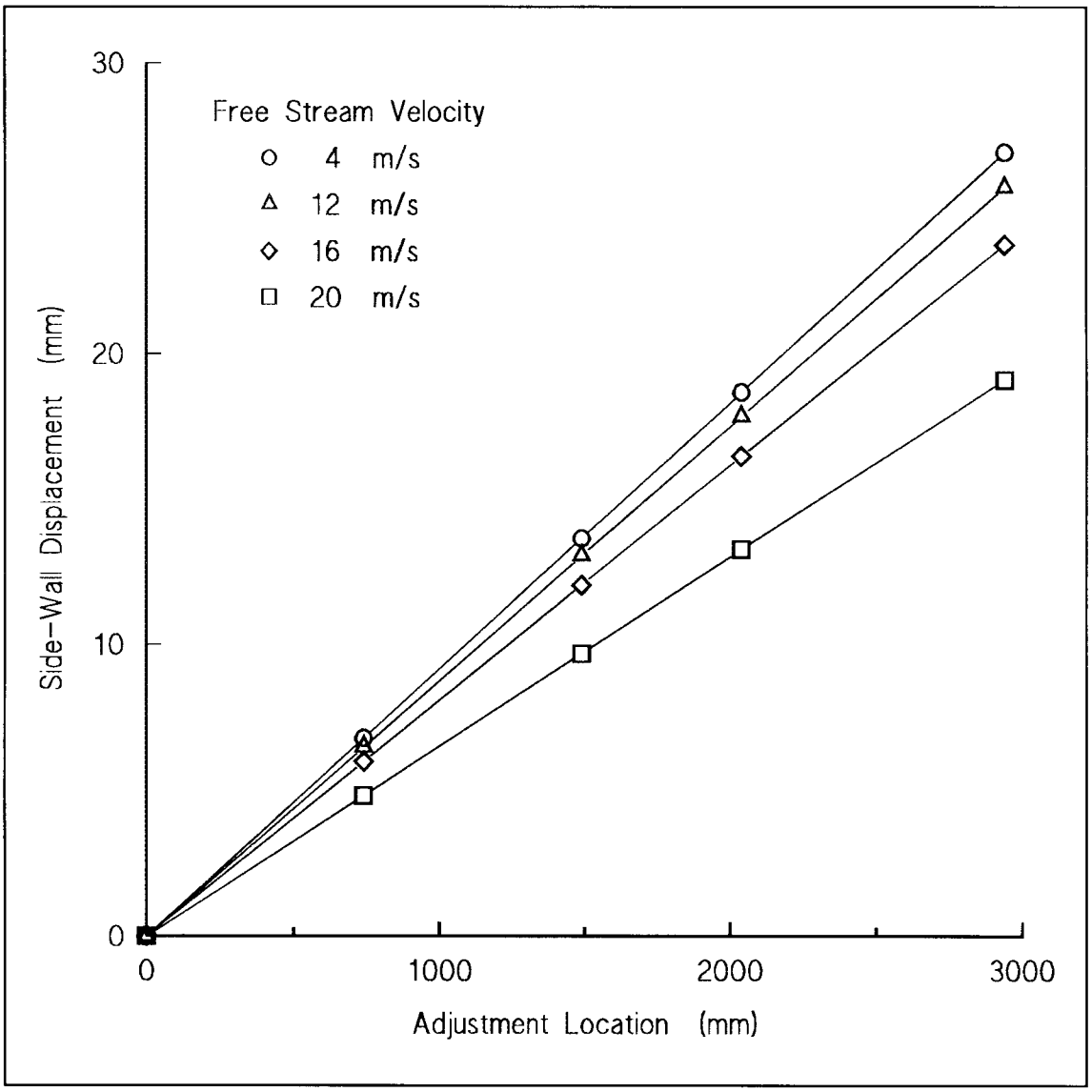

Figure 3.4 Side Wall Positions for Zero Velocity Gradient.

3.1.4 Test-cylinder arrangement

The circular cylinders tested consisted of lengths of nylon line, of diameter 0.90 mm, 1.93 mm and 2.95 mm. In each case the cylinder was anchored at the upstream end by wire stays in the wind tunnel contraction, and held in tension at the downstream end by means of a pulley and a weight, as shown in Figure [3.5]. The cylinder yaw angle may be varied from 0° to 12° by moving the pulley horizontally across the end of the test section, and by adjusting the lengths of the upstream supports.

For axial flow, the test cylinder was initially aligned relative to the test section walls. Final alignment was achieved by measuring the boundary layer velocity profile on either side of (and above and below) the cylinder, and making incremental adjustments to the upstream supports until boundary layer symmetry was achieved. In all cases the initial geometrical alignment was found to have been within 0.1° of the final alignment. For near axial flow cases the cylinder yaw angle was determined by measuring the cylinder's horizontal displacement from the axial alignment position using a micrometer surface gauge with a resolution of 0.01 mm.

The frequency of natural vibration of the test cylinders can be varied by altering the tension by adding incremental weights to the initial 5kg weight. This enabled the natural frequency to be separated from any fluid related forcing frequency. These adjustments were performed whenever the measured periodic velocity variations in the flow were observed to lock on to a single frequency (a vibration harmonic) rather than to vary about a mean fluid frequency; such adjustments can be made without the need to calculate the cylinders natural frequency and harmonics.

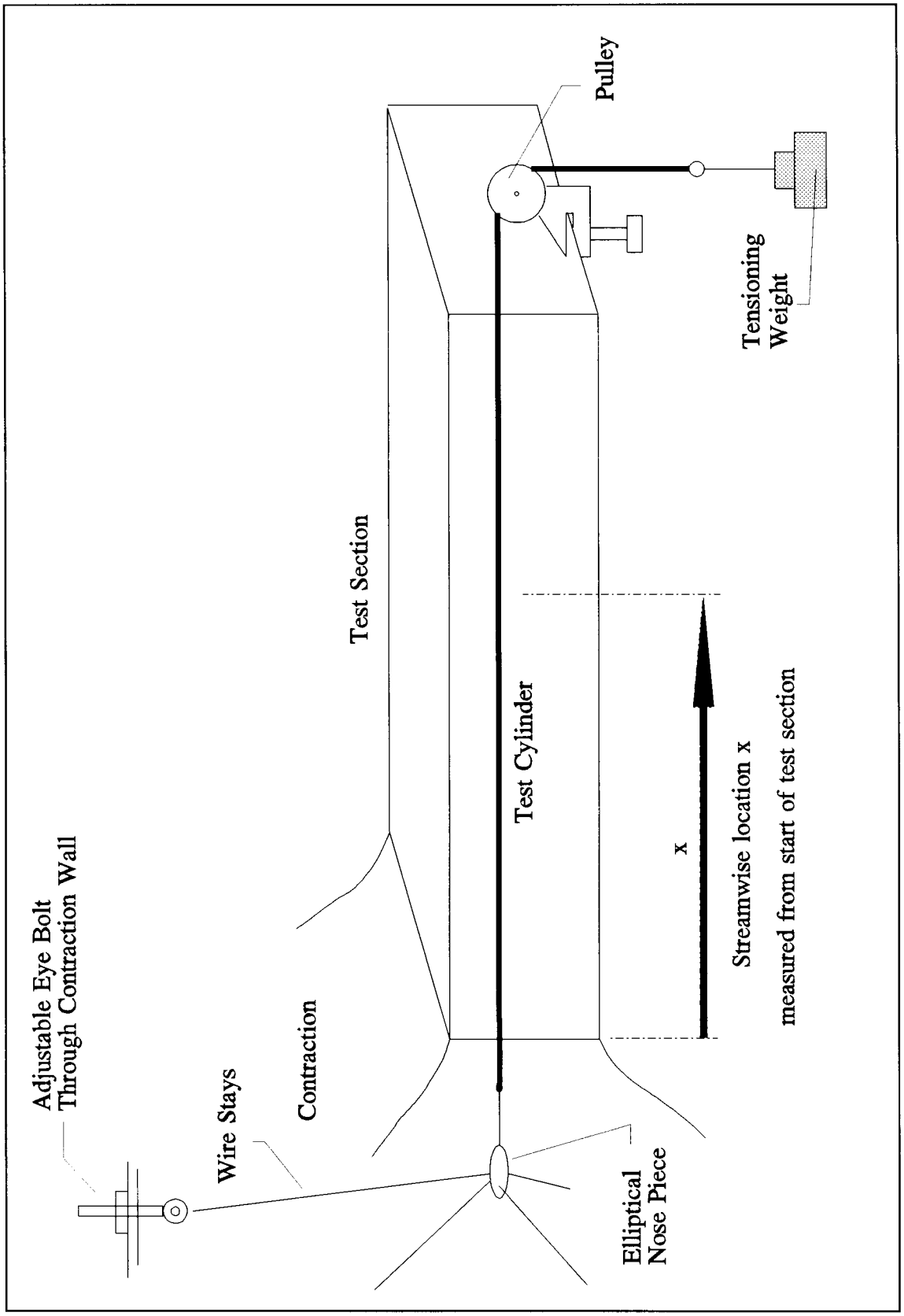

Figure 3.5 Test Cylinder End Supports.

3.2 Flow Visualisation in Air

Visualisation of the air flow is achieved by means of smoke produced by the vaporisation of a film of oil from an electrically heated wire. Two arrangements of such 'smoke wires' were used in the wind tunnel test section. A single smoke wire (shown in Figure [3.6]), positioned vertically through the test section, and passing adjacent to the test cylinder, is coated with oil which forms into regularly spaced beads along the wire. An electric current is used to heat the wire, causing the beads of oil to vaporise and form regularly spaced streamlines of smoke. The oil coating is applied to the wire by pulling the wire through an oil reservoir located on top of the test section. The wire is held straight by small tensioning weights as shown in Figure [3.6]. The smoke streaks were illuminated by spotlights and filmed on video.

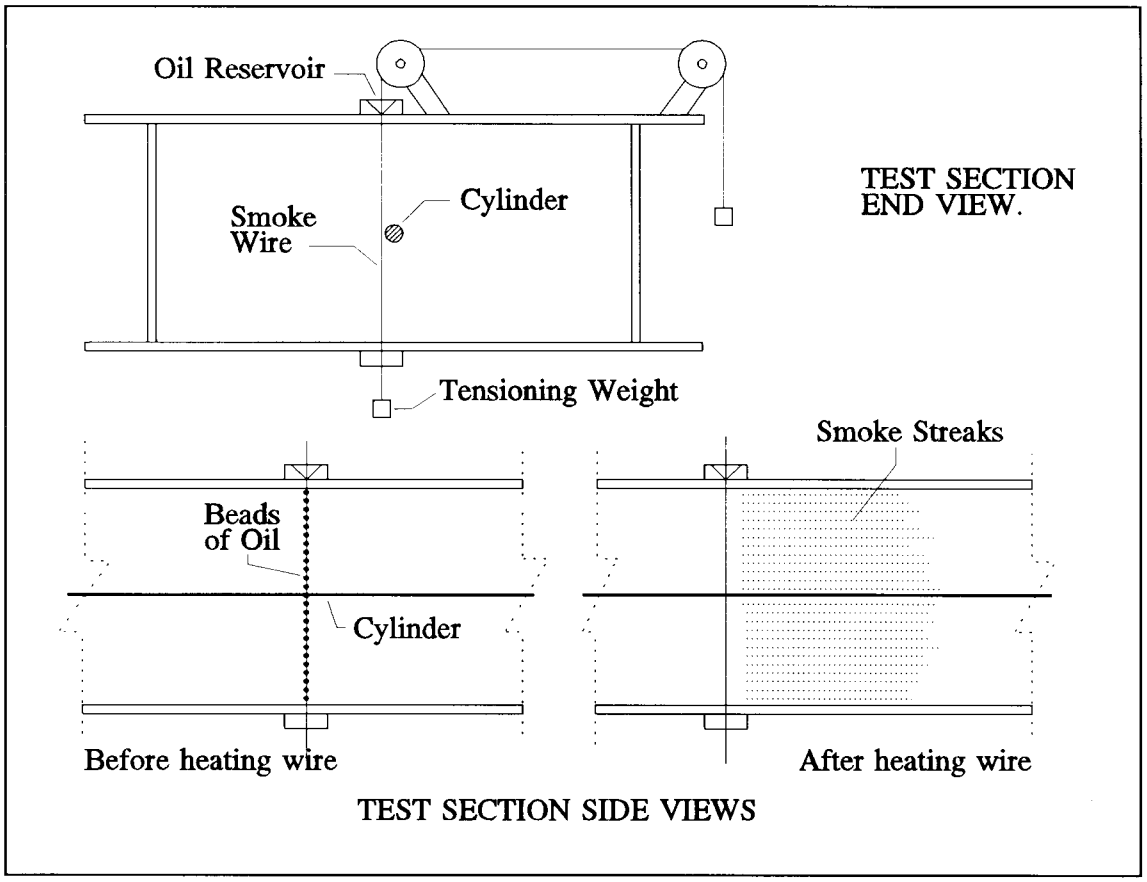

Figure 3.6 Vertical Smoke Wire.

Two video systems were used, a conventional 25 frame/second VHS system, and a high speed Kodak Ekta Pro video system capable of recording 1000 frames/second. The limited amount of light reflected by the smoke particles restricted the use of the high speed system to less than 100 frames/second.

A second smoke wire arrangement, shown in Figure [3.7], is used to generate smoke from the surface of the test cylinder. A ceramic insert in a hollow 2.95 mm diameter cylinder is wound with resistance wire which may be electrically heated by a power connection through the centre of the downstream cylinder length. An oil coating is applied manually with a small artist's-paint-brush. The lighting and video recording arrangements are similar to those for the vertical smoke wire with the addition of a mirror arranged to direct some of the camera's field of view to an oscilloscope screen displaying the voltage output from a hot-wire anemometer.

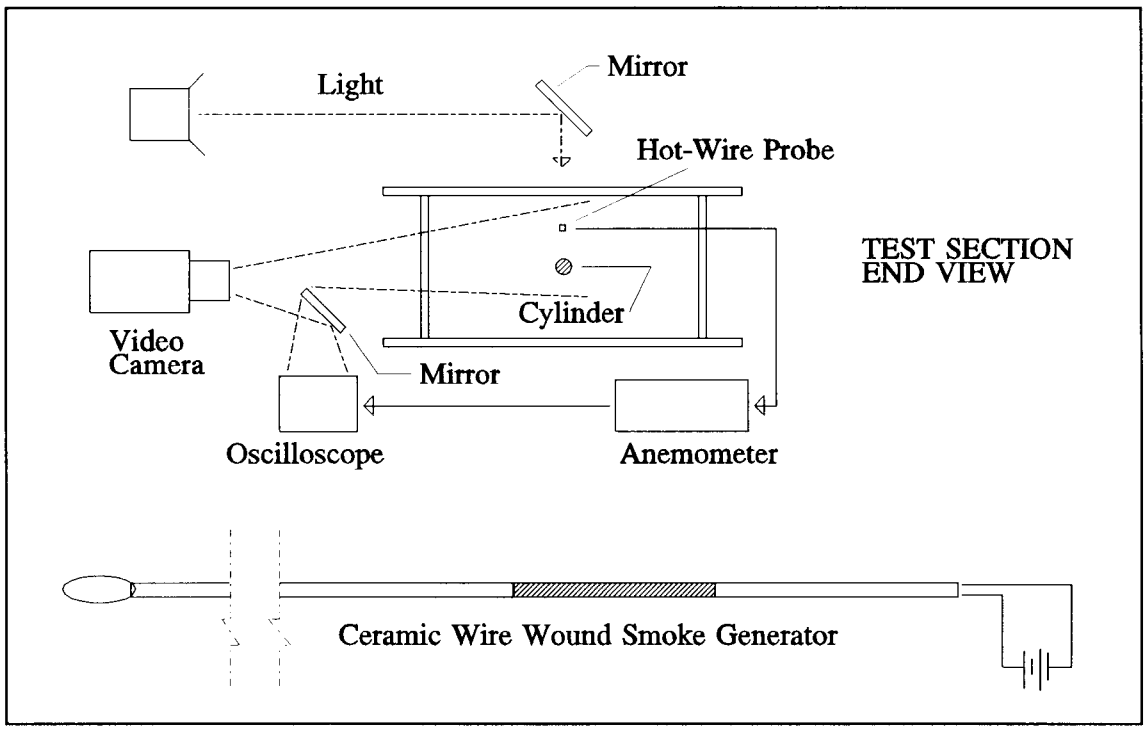

Figure 3.7 Surface Smoke Generation with Simultaneous Hot-Wire Anemometry.

3.3 Hot Wire Anemometry

A four channel TSI IFA-100 constant temperature hot wire anemometer with an overheat ratio set to 1.8 was used for velocity measurements in the air flow. The voltage output may be either the total DC voltage or the fluctuating AC component. In the DC mode a range of time constants are available (low pass filters) to produce time averages of the mean voltage output. The frequency response of each anemometer channel may be adjusted by varying the bridge and cable compensation while viewing the output voltage response to an inbuilt square wave generator.

Identical signal conditioners are available for each anemometer, allowing the output voltage to be offset, amplified and filtered while maintaining time correlation between channels. The offset may be set in one volt increments between 0 and 9 volts. The gain may be set between 1 and 900 as a single digit mantissa (1 - 9) and an exponent of 0, 1 or 2. The filter is a third-order Sallen-Key type (-18dB/octave), with a low pass setting range from 1 Hz to 400,000 Hz entered as a single digit mantissa and an exponent of 0 through 9.

A horizontal traverse system was constructed to support two micrometer surface gauges (reading $\pm$ 0.01 mm), which were used to position the hot-wire probes in the vertical direction as shown in Figure [3.8].

The location of the probes relative to the cylinder surface was determined optically by means of a small telescope (with cross hairs), clamped to a vertical

column. The telescope height may be adjusted coarsely by varying the clamping position, and very precisely over a 10 mm range by a vernier micrometer (also shown in Figure [3.8]). Vertical displacements may be measured to an accuracy of ± 0.05 mm by aligning the telescope so that the cross hairs intersect on the active length of the hot wire probe, setting the vernier scale to zero, and then adjusting the micrometer until the cross hairs intersect on the cylinder surface.

When two probes are used together, the vertical displacement between them may be measured in a similar manner. The horizontal displacement between them may be determined by initially optically aligning the probes in the vertical direction, and then measuring subsequent displacements of the horizontal traverse using a pair of vernier callipers.

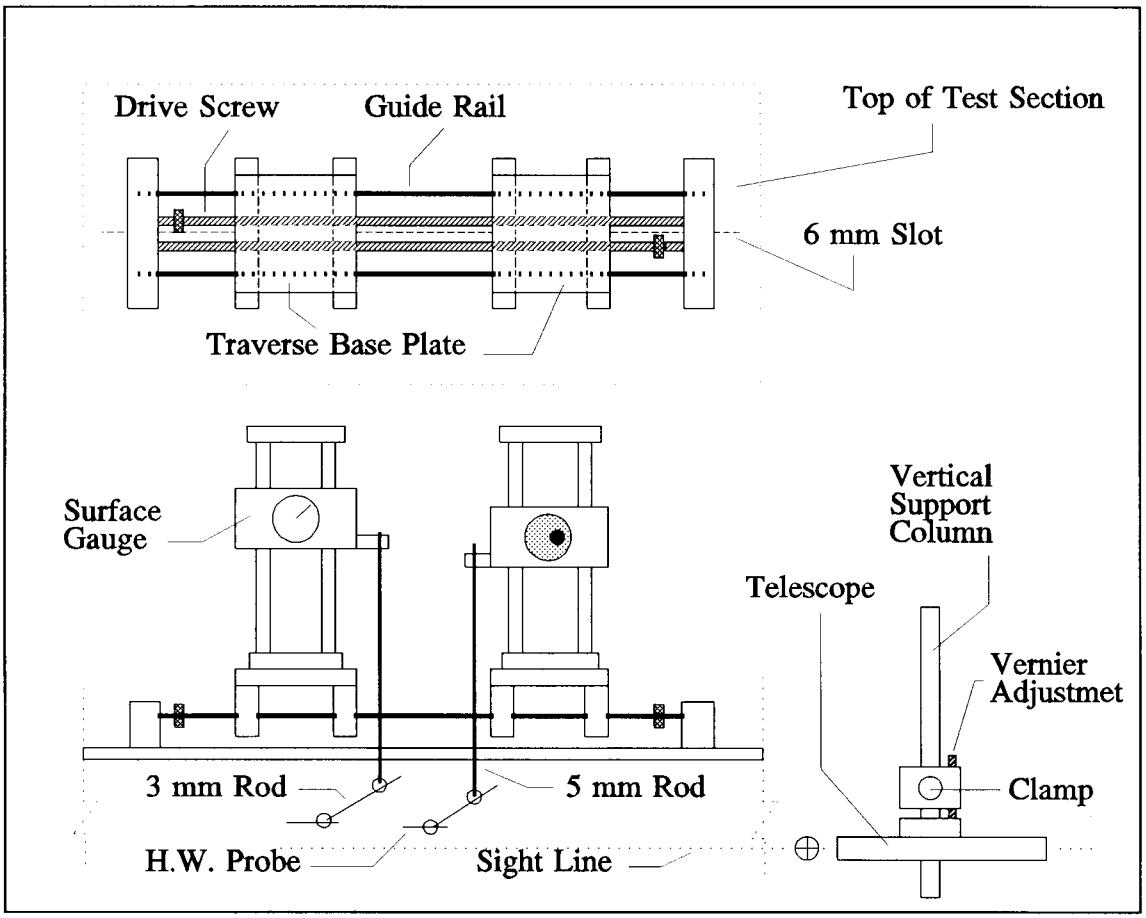

Figure 3.8 Hot Wire Probe Positioning Traverse and optical alignment system.

3.3.1 Probe design

For velocity measurements in the free stream, or in the outer boundary layer, the u-component (streamwise component) is measured using a 4μm-diameter tungsten wire with an active length of 1 mm, giving a length to diameter ratio of 200, and a typical cold resistance of 6.5 Ohms. Two probe designs were used, a straight probe shown in Figure [3.9(a)], and a 90° angled probe shown in Figure [3.9(b)]. In both these probe designs the ends of the tungsten wire are copper coated, and then soft soldered to the ends of steel needles supported in a two core ceramic rod.

For u-component velocity measurements close to the cylinder surface, it is necessary to minimise the active length of the probe in order to minimise the variation in y (distance to the surface) along the active length of the probe due to the transverse curvature of the cylinder surface. In the inner boundary layer, a straight probe with a 0.3 mm active length of 2.5 μm-diameter Wollaston wire (90% Pt, 10% Rd) is used, giving a length to diameter ratio of 120. The probe construction is shown in Figure [3.9(c)], and is similar to that of the straight tungsten wire probe except that the hot wire projects forward of the ends of the supporting needles, allowing for greater accuracy in optically determining the position of the active length.

For u and v-component (streamwise and radial) velocity measurements, a cross-wire probe is used with two matched-resistance, 2.5 μm-diameter Wollaston wires of active length 0.3 mm. The hot wires are soft soldered to steel needles held in a four core ceramic rod, with the protruding ends inclined at 45° to the rod as shown in Figure [3.9(d)].

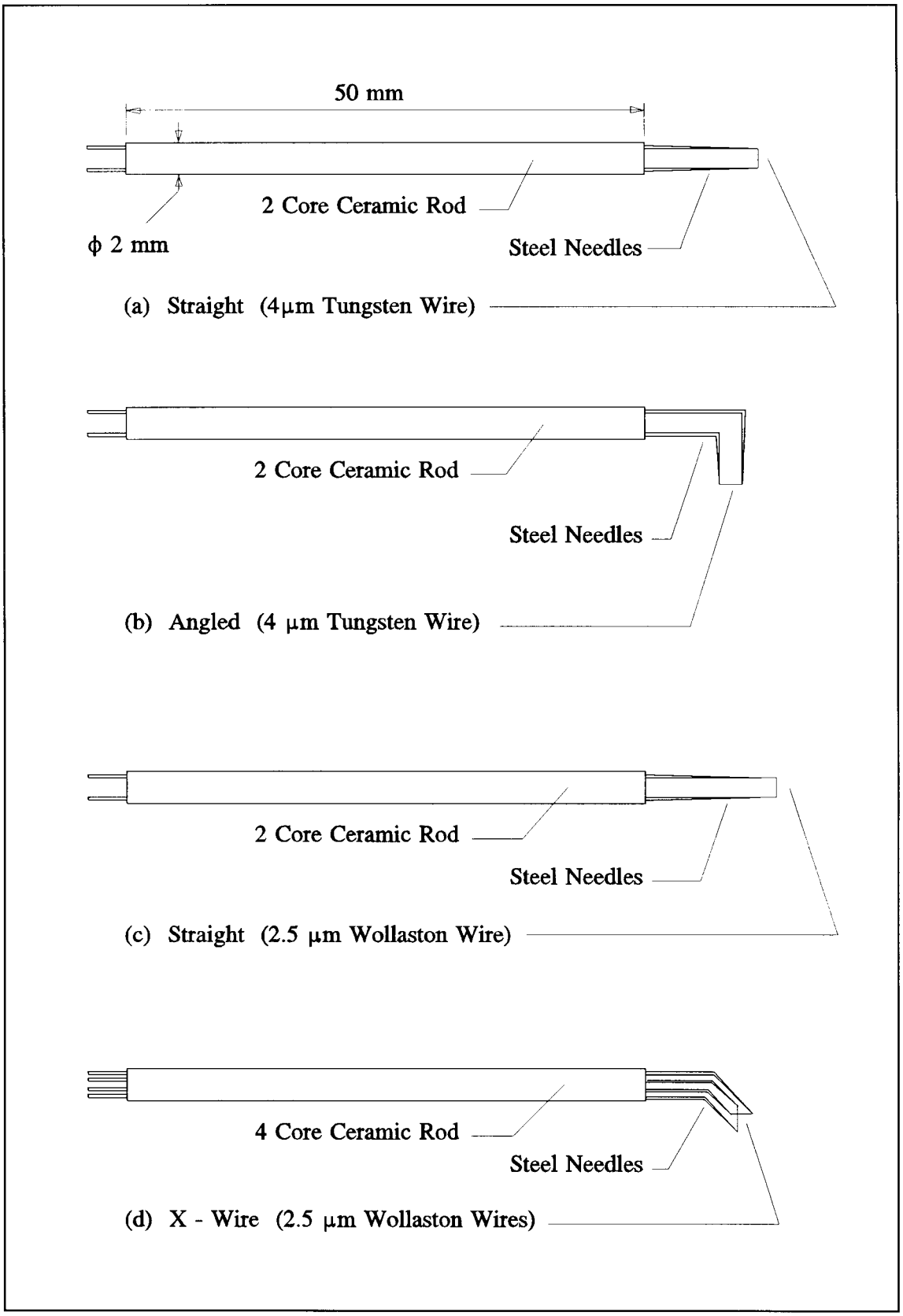

Figure 3.9 Hot Wire Probe Design.

3.3.2 Calibration

The single hot wire probes (u velocity component), were calibrated in the wind tunnel test section against a Pitot-static tube. In each calibration five velocities (U) and the corresponding voltages (E) were recorded, and the linear calibration constants A and E_0^2 obtained in the form:

$$U^{0.45} = E_0^2 + A.(E)^2 \qquad [3.4]$$

The X-wire probes were calibrated by recording the velocity and voltage output from each wire for five velocities. The calibration procedure followed the method of Bradshaw (1971), using a simple cosine law for the effect of wire inclination ψ (measured from the wire axis to the direction normal to the flow), in the form

$$U_{eff} = U.\mathrm{Cos}\ \psi \quad . \qquad [3.5]$$

The effective cooling velocity of each wire is a function of the normal velocity component only, and the cooling effects of the longitudinal velocity component are allowed for by calculating an effective wire angle ψ_{eff} determined by a yaw calibration.

The probe output is recorded for five velocities at each of five yaw angles $\Delta\psi$ equal to 0°, ± 2.5° and ± 5° as shown in the standard linear form in Figure [3.10(a)]. The yaw angles are determined optically by measuring the rotation required to align the telescope cross-hairs with the hot wire probe. The effective wire angle is calculated by plotting the output voltage E of each wire in the form

$$\left[\frac{E^2-E_0^2}{(E^2-E_0^2)_{\Delta\psi=0}}\right]^{\frac{1}{0.45}} - \cos\Delta\psi \equiv -\tan\psi_{eff} \,.\, \sin\Delta\psi \qquad [3.6]$$

against $\sin\Delta\psi$ as shown in Figure [3.10(b)].

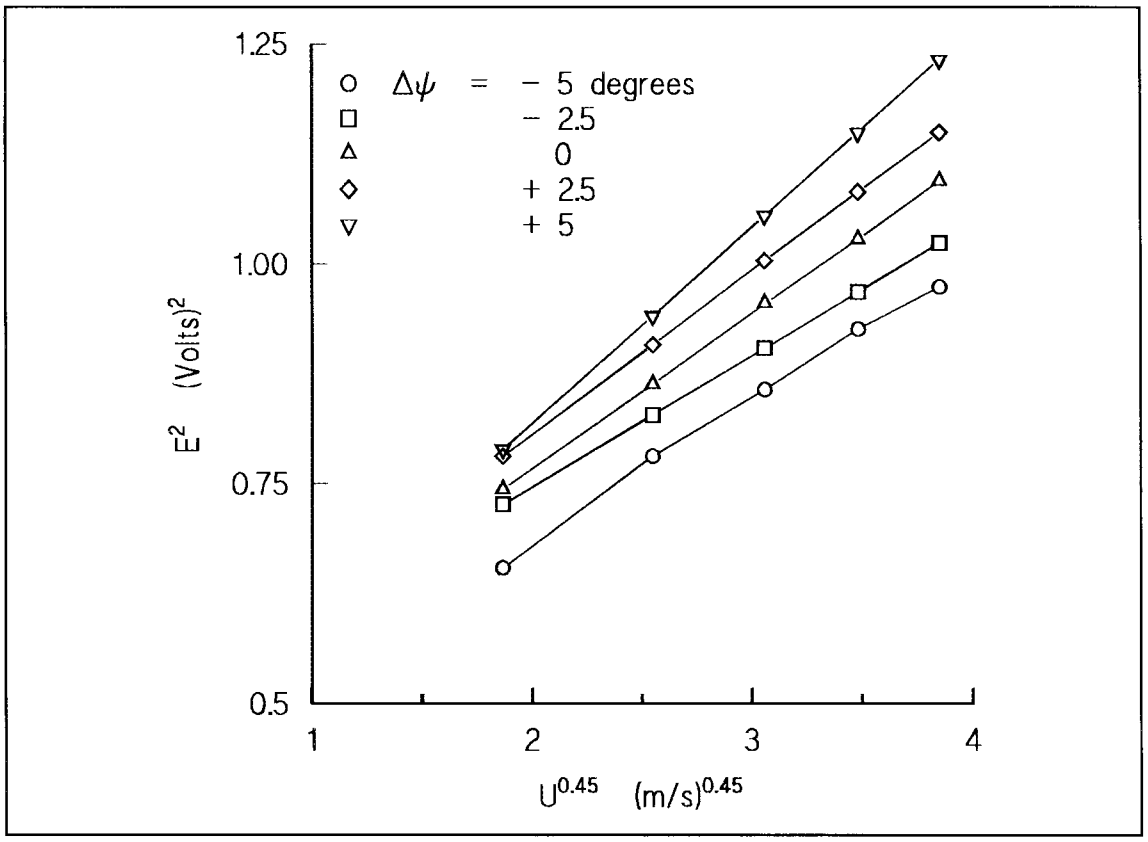

Figure 3.10(a) Calibration lines for one member of a X-Wire pair.

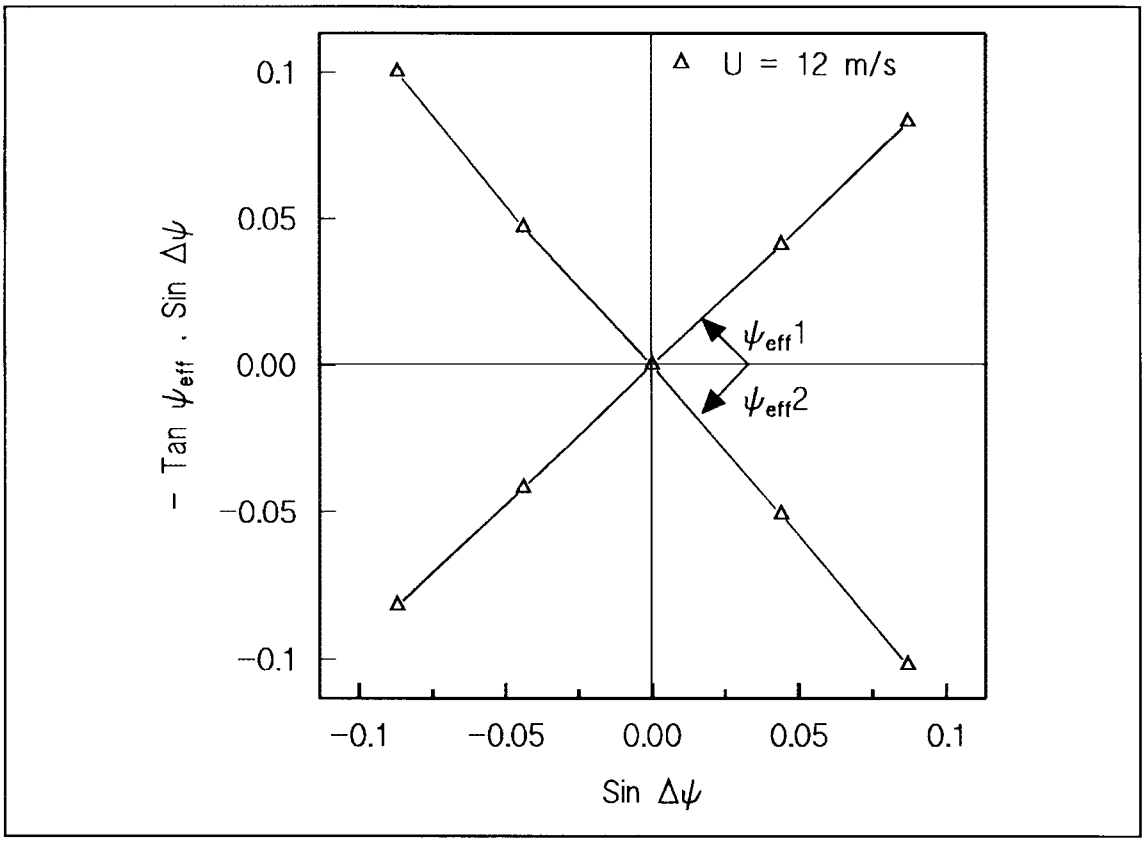

Figure 3.10(b) Yaw Calibration to determine effective yaw angle ψ_{eff}.

3.3.3 Digital data acquisition

After filtering the IFA-300 anemometer output voltage at 10 kHz, the analogue data were digitised by either of two methods. In the first method the anemometer output voltage is digitised by both a Hewlett-Packard-3582A Spectrum Analyser and a Phillips PM 3310-60 MHz digital storage oscilloscope as shown in Figure [3.11(a)]. In the second method the filtered anemometer output voltage is digitised by an RTI-860 analogue-to-digital converter at 20 kHz, and the digitised data recorded by an 80386 micro processor as shown in Figure [3.11(b)]. Up to four channels of anemometer output voltage may be digitised simultaneously using this method, and the 80386 processor is then used to convert the voltage data to velocity data using the appropriate calibration information, and to perform any subsequent data analysis.

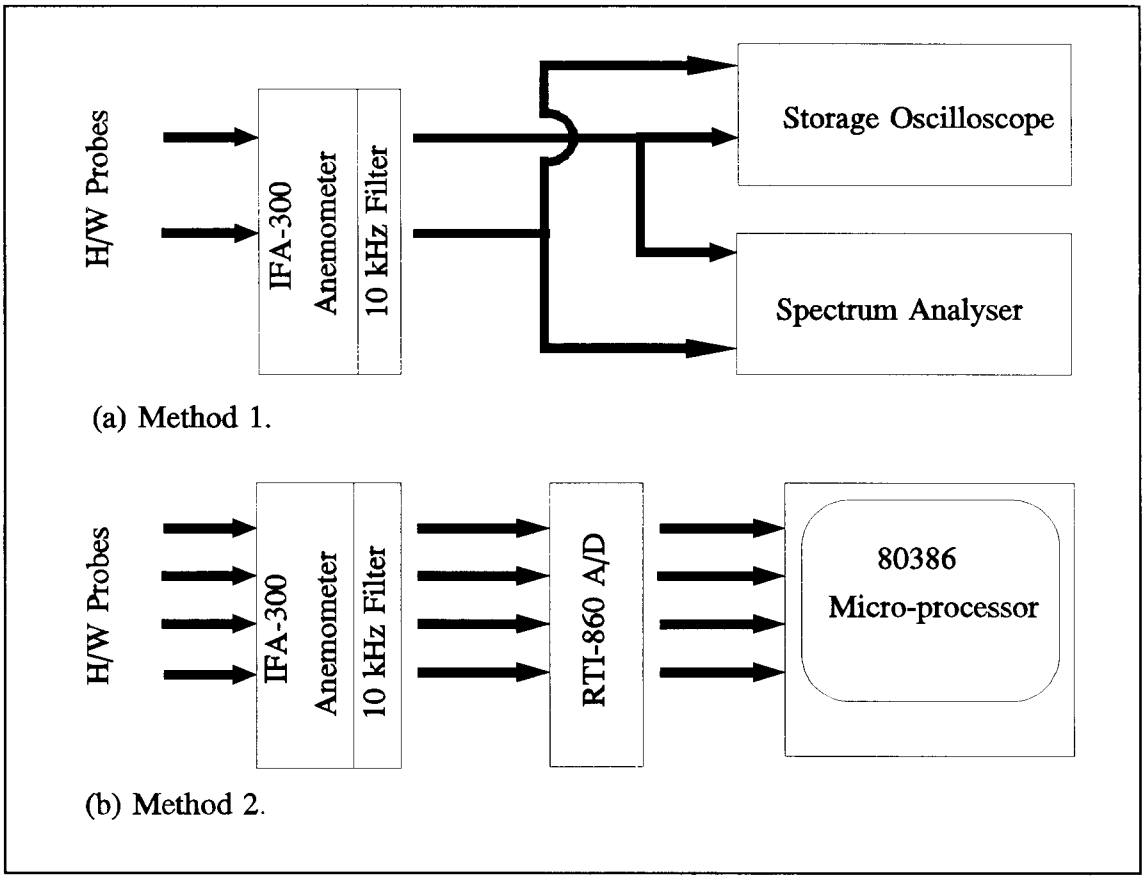

Figure 3.11 Digital Data Acquisition

3.4 Recirculating Water Tunnel

A recirculating water tunnel, shown in Figure [3.12], was designed and constructed for hydrogen-bubble flow-visualisation. The working section of the tunnel consisted of a 3.5 metre long open-topped perspex channel 475 mm deep and 175 mm wide, filled with water to a depth of 450 mm. The flow quality was controlled by a settling chamber 700 mm wide and 475 mm deep, followed by a honeycomb section, two wire screens and a 4:1 two-dimensional horizontal contraction, all separated by appropriate settling lengths.

These components were designed by adapting the low-speed-wind-tunnel design criteria established by Pankhurst and Holder (1952), Bradshaw and Pankhurst (1964) and Mehta and Bradshaw (1979) to the use of water as the working fluid. Suitable stainless steel mesh screens were selected, based on the calculation of the flow resistance by the method of Wieghardt (1953). The honeycomb section was constructed by securing an array of short plastic drinking straws between two wire screens; it was designed so that the resulting honeycomb cell dimensions would produce maximum net turbulence suppression, based on the calculation of turbulence suppression and generation by the method of Loehrke and Nagib (1976). The two dimensional contraction was designed using the two-cubic-arc method given by Morel (1977) to maximise uniformity of velocity across the section while minimising the contraction length, and hence minimising the wall boundary layer thickness at the contraction exit.

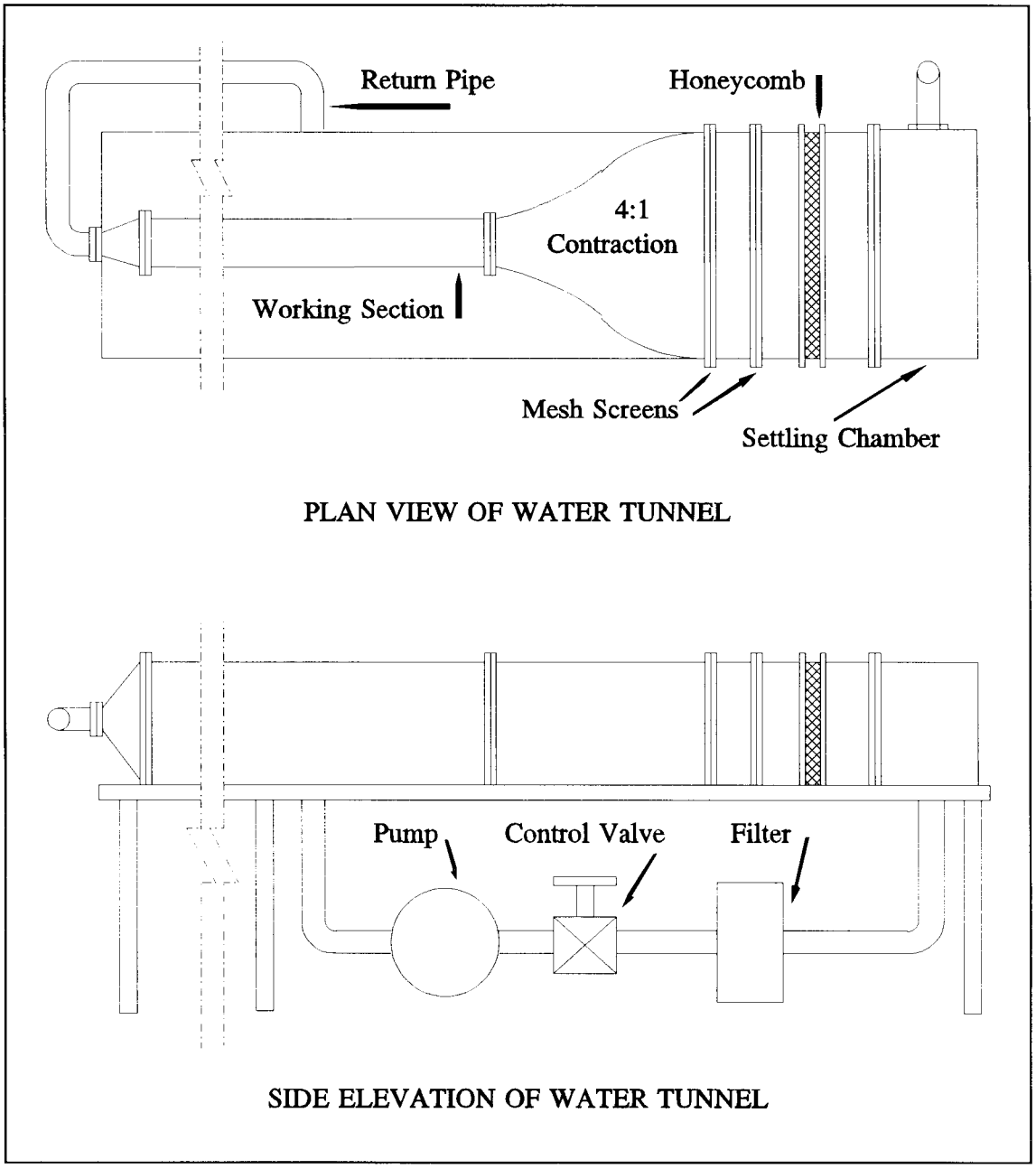

Figure 3.12 Recirculating Water Tunnel.

The water was recirculated by a constant speed centrifugal pump through a 150 mm-diameter PVC pipe return circuit. The flow velocity was controlled by means of a 150 mm-diameter gate valve located at the pump outlet. The water quality was maintained by an inline porous filter, and by treating the water with a commercial swimming pool algicide.

3.4.1 Free stream velocity

A maximum free stream velocity of 0.23 m/s within the working section of the water tunnel is obtained when the flow control valve is fully open. Partial closure of the valve enables the flow velocity to be decreased to any required value below the maximum.

The maximum flow velocity attainable gives cylinder Reynolds numbers of the same magnitude as those in the wind-tunnel test-section at low wind speeds, for the same cylinder dimensions.

The water velocity is determined by timing the passage of hydrogen bubbles past markers on the working-section side-walls using a stopwatch. This method has a limited accuracy of $\pm$ 5% due to the variation in the response time of the stopwatch operator.

The water tunnel is located within the same laboratory as the low speed wind tunnel, and the laboratory air-conditioning system is used to maintain a constant ambient air temperature of 21° C in order to hold the water density ρ_w and viscosity μ_w constant at

$$\rho_w = 997.5 \text{ kg/m}^3$$

$$\mu_w = 0.98 \times 10^{-3} \text{ kg/m.s} \quad .$$

3.4.2 Test cylinder arrangement

The circular cylinders used in the water tunnel were similar to those used in the low speed wind tunnel, consisting of lengths of nylon line of diameter 0.90 mm, 1.93 mm and 2.95 mm. Each test cylinder is supported at its upstream end within the tunnel contraction by three wire stays which pass through the turbulence-reducing screens to anchor points on the tunnel walls as shown in Figure [3.13]. The downstream end of the test cylinder is hand tensioned through a hole in the downstream support post, shown in Figure [3.13], and secured in place by a small grub screw. The slight elastic elongation of the test cylinder is sufficient to prevent the cylinder from sagging under its own weight. Potential sagging is also greatly decreased by the buoyancy forces along the length of the submerged cylinder.

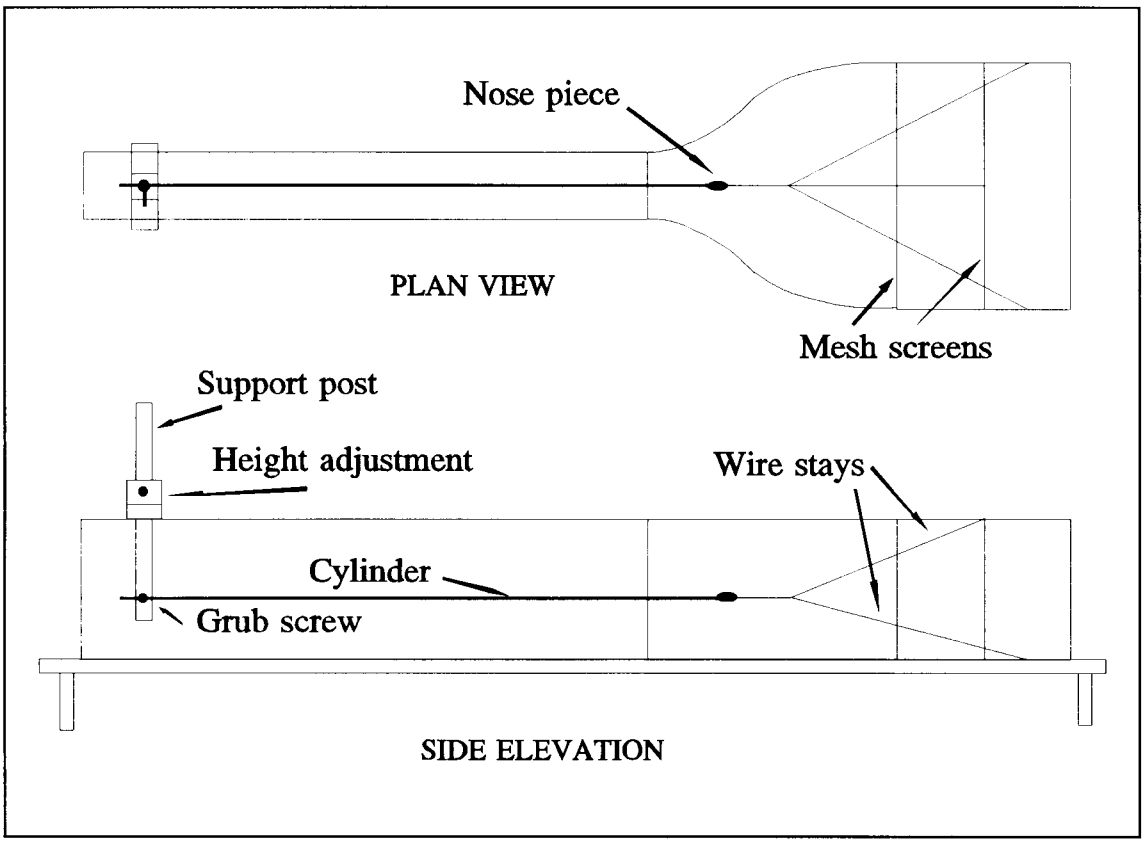

Figure 3.13 Test cylinder arrangement.

3.5 Hydrogen-bubble Flow Visualisation

The technique of flow visualisation by the electrolysis of water is now a well established method (Merzkirch 1987) of visualising the velocity field in a water flow using bubbles of hydrogen to mark the fluid. The method is described in detail by Clutter and Smith (1961), based on initial work by Geller (1954), with a more quantitative analysis of the technique given by Schraub et. al. (1965) and by Davis and Fox (1967).

The electrolysis process is controlled by an adjustable Direct Current power supply capable of generating a potential of up to 75 Volts between two electrodes in the water flow. The anode used is a 4 mm diameter stainless steel rod suspended in the water flow downstream of the area to be investigated. The cathode consists of a length of 100 μm-diameter steel wire tensioned between two insulated 4 mm-diameter stainless steel supports at the upstream end of the area to be visualised.

The various cathode geometries used are shown in Figure [3.14], the bubble generating wire being either straight or kinked. The kinked wire is made by drawing a length of straight wire between two small intermeshed gear wheels, producing a series of kinks in the wire at approximately 2 mm spacing. The advantage of the kinked wire over the straight wire is its production of a series of distinct, evenly spaced lines of hydrogen bubbles rather than the continuous sheet of bubbles produced by a straight wire, as a result of the bubbles being swept along each kink to its downstream point before leaving the wire.

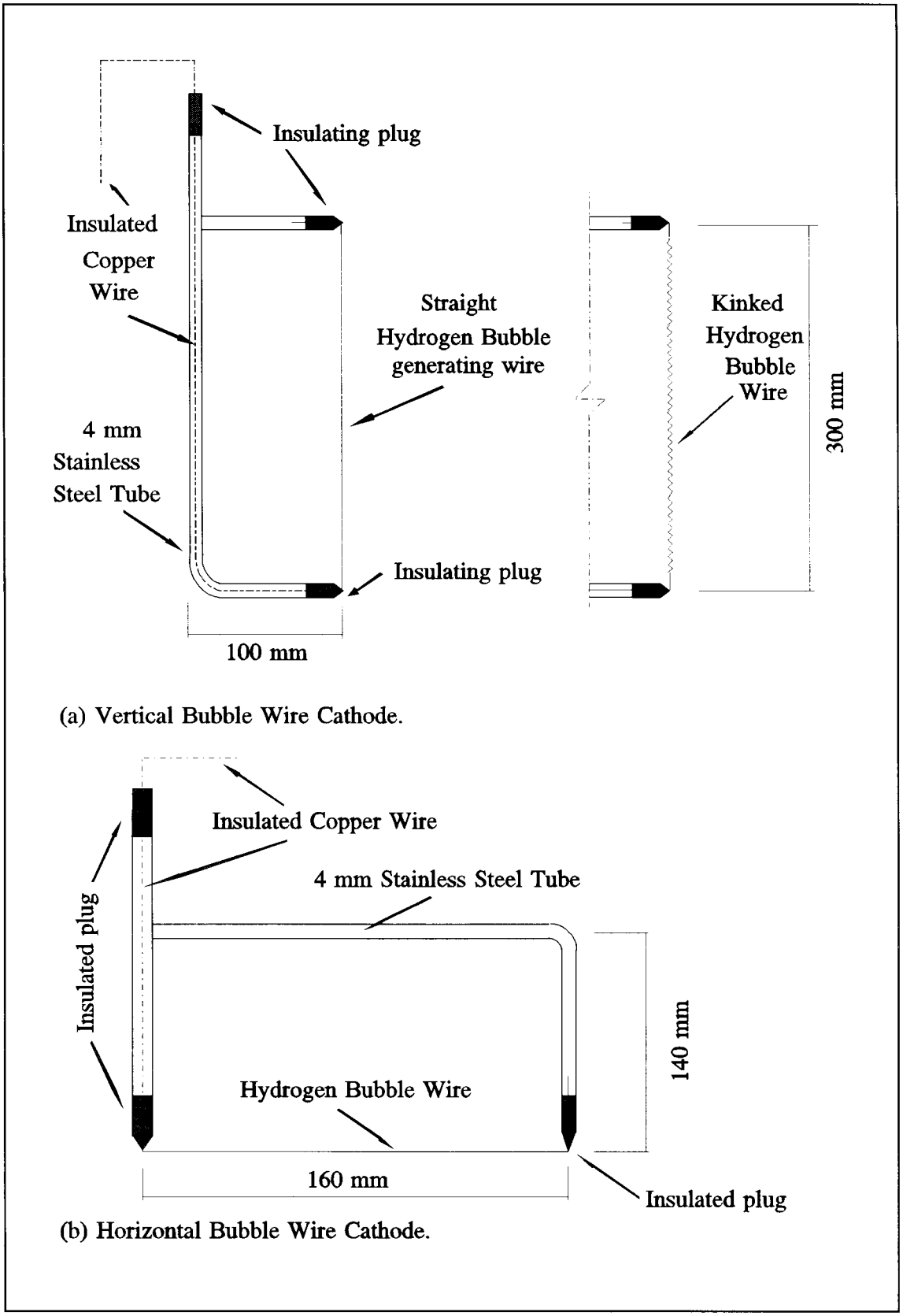

Figure 3.14 Hydrogen Bubble Wire Cathodes.

The various physical arrangements of the bubble-generating wire and the test cylinder are shown in Figure [3.15]. As the cylinder is yawed in the vertical plane, the vortex wake of the cylinder is also in the vertical plane. This arrangement of a yawed cylinder produces a wake similar to that of a vertical cylinder normal to the flow; a vertical view will illustrate the vortices as a series of spirals while a horizontal view will illustrate them as a series of lines, and therefore two basic visualisation arrangements are used. In the first arrangement shown in Figure [3.15(a)] a vertical bubble wire is used in conjunction with a vertical sheet of light. In a horizontal view through the side walls of the water-tunnel working-section, the rolled-up vortex cores in the cylinder wake then appear as a series of lines which indicate the orientation of the vortex axes relative to the cylinder and to the flow.

In the second arrangement shown in Figure [3.15(b)] a horizontal bubble wire is used in conjunction with a horizontal sheet of light so that in a vertical view down through the water surface the vortices are seen end-on as contracting spirals. A perspex plate suspended on the water surface is used to remove any surface ripples present in the free surface which might otherwise distort the image of the hydrogen bubbles below the surface.

The images of the velocity field thus produced were recorded by both video (25 frames per second), and by still photography (35mm camera). The sheets of light used to illuminate the hydrogen bubbles are produced by two fan-cooled light-boxes with adjustable-width slits to emit the light produced by 150 Watt halogen lamps. A matt black background to the flow is produced by the addition of a flat plastic sheet to the inside of the working section floor or rear wall as required.

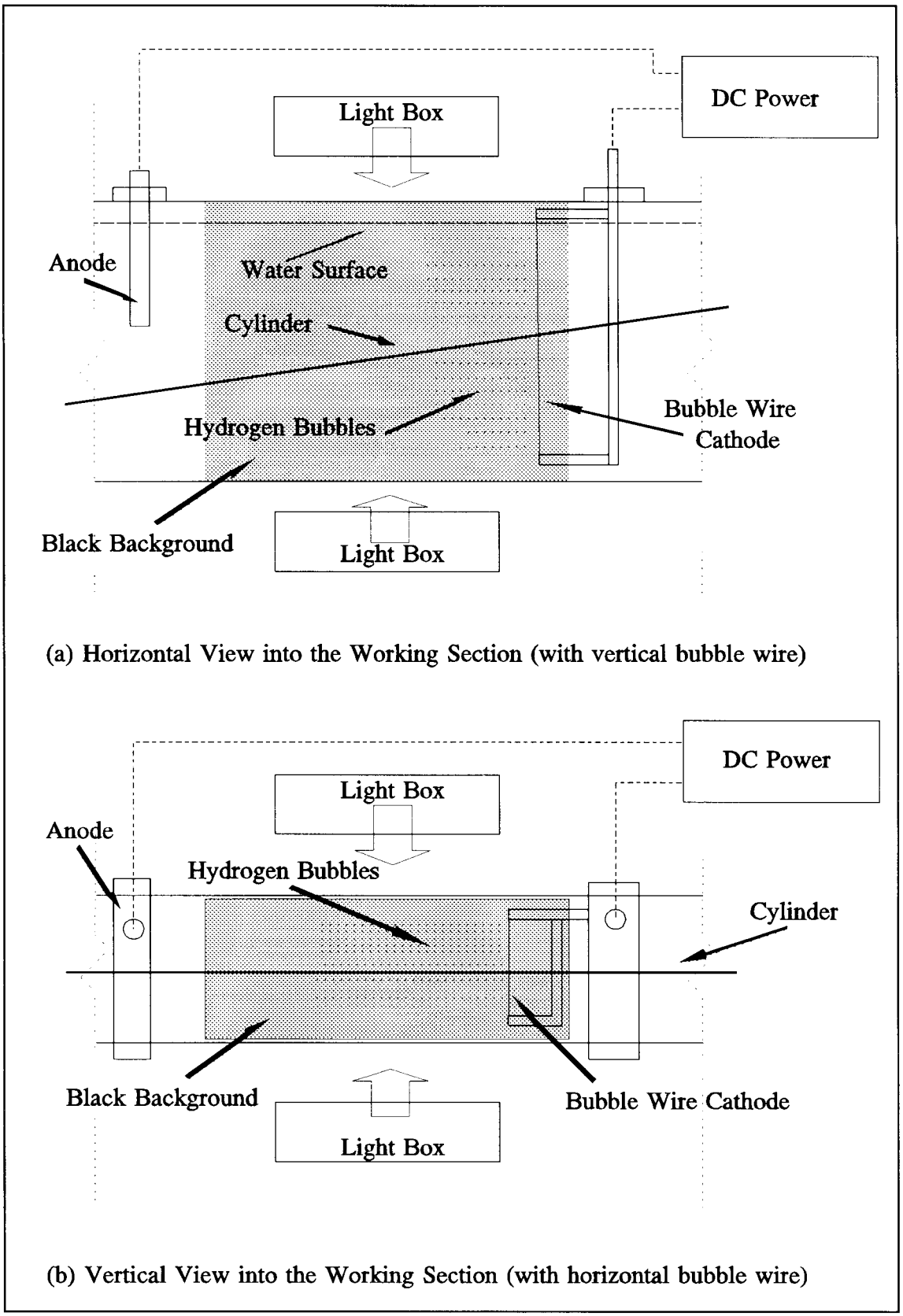

Figure 3.15 Hydrogen Bubble Flow Visualisation Arrangement.